The Src and Abl family kinases activate the Spleen Tyrosine Kinase to maximize phagocytosis and *Leishmania* infection

Running title: *SYK mediates Leishmania infection*

Imran Ullah[1, 2, #], Umaru Barrie[1, 3], Rebecca M. Kernen[1,4], Emily T. Mamula[1], Francis Tho Huu Khuong II[1, @], Laela M. Booshehri[1,^], Emma L. Rhodes[1], James M. Bradford[1,+], Arani Datta[1], and Dawn M. Wetzel[1, 2*]

[1]Department of Pediatrics, University of Texas Southwestern Medical Center, 5323 Harry Hines Blvd, Dallas, Texas, 75390, United States. [2]Department of Biochemistry, University of Texas Southwestern Medical Center, 5323 Harry Hines Blvd, Dallas, Texas, 75390, United States. [3]Medical Scientist Training Program, University of Texas Southwestern Medical Center, 5323 Harry Hines Blvd, Dallas, Texas, 75390, United States. [4]Emergency Medicine Residency Program, University of Texas Southwestern Medical Center, 5323 Harry Hines Blvd, Dallas, Texas, 75390, United States

*Corresponding author: Email: dawn.wetzel@utsouthwestern.edu

[#]Present Address: Department of Immunology and Infectious Diseases, Harvard T.H. Chan School of Public Health, Boston, MA 02115, USA

^Present Address: Doctoral Program, Scripps Institution of Oceanography, UC San Diego, La Jolla, CA, 92093

[+]Present Address: Dell Medical School, UT Austin, Austin, TX, 78712

[@]Present Address: M.D./Ph.D. Program, Texas Tech University Health Sciences Center, Lubbock, TX, 79430

Keywords: *Leishmania*, kinase, pathogen, parasite, macrophage

Abbreviations: BMDM, bone marrow-derived macrophages; C3bi, terminal component of complement; CR3, complement receptor 3; FcR, Fc receptor; h, hour; IgG, immunoglobulin G; LPS, lipopolysaccharide; Mϕ, macrophage; m, minutes; SE, standard error; p-, phosphorylated; SFK, Src family kinases; SYK, spleen tyrosine kinase

SUMMARY STATEMENT

Activation of Spleen Tyrosine Kinase by Src and Abl family kinases is required for maximal *Leishmania* uptake by macrophages and disease in a mouse model of cutaneous leishmaniasis.

ABSTRACT

Leishmania spp. are obligate intracellular parasites that must be internalized by phagocytic cells to evade immune responses and cause disease. The uptake of both *Leishmania* promastigotes (insect-stage parasites) and amastigotes (proliferative stage parasites in humans and mice) by phagocytes is thought to be mainly host cell-driven, not parasite-driven. Our previous work indicates that host Src and Abl family kinases facilitate *Leishmania* entry into macrophages and pathogenesis in murine cutaneous leishmaniasis. Here we demonstrate that host spleen tyrosine kinase (SYK) is required for efficient uptake of *Leishmania* promastigotes and amastigotes. A Src family kinase-Abl family kinase-SYK signaling cascade induces *Leishmania* amastigote internalization. Finally, lesion size and parasite burden during *Leishmania* infection is significantly decreased in mice lacking SYK in monocytes or by treatment with the SYK inhibitor entospletinib. In summary, SYK is required for maximal *Leishmania* uptake by

55 macrophages and disease in mice. Our results suggest potential for treating
56 leishmaniasis using host cell-directed agents.
57

58 **INTRODUCTION**

59 Approximately 350 million people worldwide are at risk for the disfiguring
60 cutaneous or fatal visceral forms of leishmaniasis, which is a neglected tropical disease
61 (WHO, 2022). The drugs currently used to treat leishmaniasis have poor efficacy and/or
62 are highly toxic to human hosts; therefore, new antiparasitics are urgently needed (Wetzel
63 and Phillips, 2018). Leishmaniasis results from infection by obligate intracellular parasites
64 in the *Leishmania* genus. During its life cycle, *Leishmania* alternates between
65 promastigotes, found in sand fly vectors, and amastigotes, found in vertebrate hosts such
66 as humans, dogs, and rodents. In order for infection to be established in humans after a
67 sand fly bite, phagocytic cells (*e.g.*, neutrophils, macrophages [Mϕ]) must ingest
68 promastigotes, using a process that is thought to be primarily driven by the host cell (Ueno
69 and Wilson, 2012). The parasites survive in acidic phagolysosomes, where they
70 differentiate into amastigotes and multiply. If amastigotes exit this compartment, they
71 must be taken up again by phagocytes to survive within their vertebrate hosts (Ueno and
72 Wilson, 2012). *Leishmania* parasites that remain outside of phagocytic cells are thought
73 to either die or be killed by the host immune system.

74

75 Multiple protein receptors on the surfaces of phagocytic cells have been implicated
76 in the process of *Leishmania* uptake. For example, promastigotes bind the complement
77 receptor CR3; this process is enhanced when parasites are opsonized (coated) with the
78 terminal component of complement, C3bi (Mosser *et al.*, 1992; Puentes *et al.*, 1988;
79 Russell and Wright, 1988). Amastigotes are opsonized with immunoglobulin G (IgG) and
80 bind the Fc receptor subclass FcγR (Guy and Belosevic, 1993), which is required for a

81 productive *in vivo* infection (Kima *et al.*, 2000). After *Leishmania* binds cell surface
82 receptors, actin-rich phagocytic cups form and surround the parasites, allowing them to
83 be internalized (Lodge and Descoteaux, 2008). However, the host cell signaling process
84 that drives *Leishmania* uptake has not been well-described.
85
86 Previously, we implicated host Src family kinases (SFK) as well as Abl family
87 kinases in the process of *Leishmania amazonensis* uptake by Mϕs. The SFK, and
88 specifically Hck, Fgr, and Lyn, are non-receptor tyrosine kinases that had been known to
89 participate in IgG-mediated phagocytosis (Fitzer-Attas *et al.*, 2000) after pathogens bind
90 the Fc Receptor (FcR) (Wu *et al.*, 2001). Using SFK inhibitors such as SU6656 and
91 primary Mϕs lacking Hck, Fgr, and Lyn, we demonstrated that SFK were necessary for
92 maximal amastigote uptake by Mϕ, as well as for disease in a mouse model of cutaneous
93 leishmaniasis (Wetzel *et al.*, 2016). SFK bind and phosphorylate another set of non-
94 receptor tyrosine kinases, the Abl family kinases Abl (Abl1) and Arg (Abl2) (Mader *et al.*,
95 2011; Plattner *et al.*, 2004; Tanis *et al.*, 2003); (Bradley and Koleske, 2009). We have
96 shown that Abl and Arg facilitate complementary activities during phagocytosis and
97 *Leishmania* uptake by Mϕ (Wetzel *et al.*, 2012). Specifically, Mϕ isolated from mice lacking
98 Arg (*Arg*$^{-/-}$ Mϕ*)* exhibited reduced phagocytosis of IgG-coated beads or amastigotes, but
99 had no defects in the uptake of C3bi-coated beads or promastigotes (Wetzel *et al.*, 2012).
100 Conversely, Mϕ from mice lacking Abl (*Abl*$^{-/-}$ Mϕ) showed defects in the uptake of C3bi-
101 coated beads and promastigotes, but had no defects in the internalization of IgG-coated
102 beads or amastigotes (Wetzel *et al.*, 2012). Mϕ lacking both Abl family kinases had no
103 deficiencies in C3bi or IgG-mediated uptake beyond that seen for Mϕs lacking the single

104 relevant kinase (Wetzel *et al.*, 2012; Wetzel *et al.*, 2016). Mice lacking Abl or Arg, or
105 treated with the Abl family kinase inhibitor imatinib, had smaller lesions and lower parasite
106 burden in a cutaneous mouse model of leishmaniasis (Wetzel *et al.*, 2012). Finally,
107 treatment of *Leishmania*-infected mice with bosutinib, which inhibits both Abl family
108 kinases and SFK, led to greater decreases in lesion size and parasite burden than were
109 seen with inhibition of either kinase family alone (Wetzel *et al.*, 2016).
110
111 Spleen Tyrosine Kinase (SYK) is a cytoplasmic tyrosine kinase with 10 tyrosines
112 that can be phosphorylated to participate in signal transduction from immune receptors
113 such as FcR (Furlong *et al.*, 1997). Mϕ derived from mice conditionally lacking SYK in
114 immune cells are defective in several FcR-induced signaling events (Bonnerot *et al.*,
115 1998; Bradshaw, 2010; Lowell, 2011). These Mϕ also have deficits in IgG-mediated
116 phagocytosis; they form actin-rich phagocytic cups but cannot close them around
117 pathogens (Crowley *et al.*, 1997). However, these Mϕ respond normally to
118 lipopolysaccharide (LPS), indicating that there are no deficiencies in activation (Crowley
119 *et al.*, 1997). Some laboratories have suggested that SYK inhibition does not affect C3bi-
120 mediated phagocytosis (Kiefer *et al.*, 1998), but others have shown significant defects in
121 this process (Tohyama and Yamamura, 2006; Walbaum *et al.*, 2021). There do not
122 appear to be SYK homologs in *Leishmania* (Baker *et al.*, 2021; Parsons *et al.*, 2005).
123
124 Prior studies suggest that kinases previously implicated in *Leishmania*
125 internalization also may modulate SYK-mediated processes in related biological systems.
126 For example, Mϕ derived from mice deficient for Hck, Fgr, and Lyn exhibited decreased

127 SYK activation when FcR was crosslinked by antibodies (Crowley *et al.*, 1997). In
128 addition, loss of Abl/Arg activity limited SYK phosphorylation after FcR crosslinking with
129 antibodies, and Arg kinase phosphorylated SYK in kinase assays with purified proteins
130 (Greuber and Pendergast, 2012). Based on these prior findings, we hypothesized that
131 host cell SYK would be activated by SFK and Abl family kinases during the uptake of
132 *Leishmania* by Mϕ, and that SYK activity would be required for pathogenesis in a mouse
133 model of leishmaniasis.
134
135 Here, we demonstrate that host cell SYK facilitates both C3bi- and IgG-mediated
136 phagocytosis and promotes the internalization of *Leishmania* promastigotes and
137 amastigotes. A SFK-Abl family kinase-SYK pathway is required for maximal
138 internalization of *Leishmania* amastigotes by Mϕ. In addition, mice lacking SYK in
139 monocytes, as well as mice treated with the SYK kinase inhibitor entospletinib, have
140 significantly reduced lesion severity and parasite burden in a mouse model of cutaneous
141 *Leishmania* infection. Our results provide proof-of-concept that leishmaniasis could
142 potentially be treated with agents directed at host cell kinases such as SYK.

143 **RESULTS**

144 **Entospletinib decreases complement and immunoglobulin-mediated phagocytosis**

145 Previously, we have shown that SFK inhibitors and Abl family kinase inhibitors
146 decrease the uptake of *Leishmania* parasites (Wetzel *et al.*, 2012; Wetzel *et al.*, 2016).
147 Others have suggested that signaling during phagocytosis by these two kinase families
148 can be relayed to SYK (Crowley *et al.*, 1997; Greuber and Pendergast, 2012). Therefore,
149 we chose to explore the role of SYK in phagocytic model systems and *Leishmania* uptake
150 by Mϕ.

151

152 Entospletinib is a SYK inhibitor that has an IC_{50} of 7.7 nM in purified kinase assays
153 (Ramanathan *et al.*, 2017). Given its recent favorable results in a human phase 1b/2 trial
154 for acute myeloid leukemia (Walker *et al.*, 2020), it is an attractive tool for further study.
155 However, its effects on phagocytosis had not been documented previously. For this
156 reason, we first determined whether entospletinib treatment of phagocytic cells affected
157 immunoglobulin-mediated phagocytosis. We treated RAW 264.7 cells, a murine Mϕ-like
158 cell line, with increasing concentrations of entospletinib or DMSO for 2 hours (h) and
159 incubated them for 30 minutes (m) with beads that had been coated with IgG. We found
160 that entospletinib, in a concentration-dependent manner, decreased the uptake of IgG-
161 coated beads, as demonstrated by the phagocytic index or number of internalized beads
162 per 100 Mϕs (PI, Fig. S1A). Based on this titration, we selected a concentration of 1 μM
163 for further studies.

164

165 Whether SYK plays a role in C3bi-mediated phagocytosis has been a subject of
166 debate (Kiefer *et al.*, 1998; Tohyama and Yamamura, 2006; Walbaum *et al.*, 2021). To
167 determine whether entospletinib treatment of host cells affected C3bi and IgG-mediated
168 phagocytosis, we treated RAW 264.7 cells with 1 μM entospletinib or DMSO for 2 h and
169 incubated them for 30 m with beads that had been coated with C3bi or IgG. We found
170 that 1 μM entospletinib decreased both C3bi-coated and IgG-coated bead uptake by RAW
171 264.7 cells by 44 ± 6% and 67 ± 8% (mean ± standard error [SE]), respectively (Fig. 1A,
172 B). Since RAW 264.7 cells are a cancer cell line that has been virally transformed, these
173 results were confirmed with primary cells: bone marrow-derived Mϕs (BMDM) isolated
174 from mouse tibias/femurs (Fig. 1C). The decreases in C3bi- and IgG-mediated
175 phagocytosis due to entospletinib treatment specifically resulted from defects in
176 internalization, as entospletinib did not affect the total (internal + external) number of C3bi-
177 and IgG-coated beads normalized to the number of RAW 264.7 cells (Fig. 1D) or BMDM
178 (Fig. 1E).
179
180 **SYK inhibition decreases *Leishmania* promastigote and amastigote uptake by Mϕs**
181 We can grow both promastigotes and amastigotes of *L. amazonensis* without
182 mammalian host cells (axenic cultures), using a supplemented growth media at pH 7.2
183 for promastigotes or pH 5 for amastigotes (Hodgkinson *et al.*, 1996). To test whether
184 entospletinib treatment also affected the internalization of promastigotes and axenic
185 amastigotes, we again pre-treated Mϕs with 1 μM entospletinib or DMSO, but now
186 incubated them with C3bi-coated *L. amazonensis* promastigotes or IgG-coated axenic
187 amastigotes. A representative image of amastigote uptake ± entospletinib is shown in Fig.

188 2A. We found that 1 μM entospletinib decreased promastigote and amastigote uptake by
189 RAW 264.7 cells (by 39 ± 3% and 54 ± 5%, respectively; Fig. 2B) and BMDM (by 49 ±
190 6% and 66 ± 6%, respectively; Fig. 2C). Titration of entospletinib demonstrated that
191 promastigote uptake and amastigote uptake by RAW 264.7 cells was decreased in a
192 concentration-dependent manner (Fig. S1B and C, respectively). Entospletinib did not
193 affect the total number of promastigotes or amastigotes that bound RAW 264.7 cells (Fig.
194 2D) or BMDM (Fig. 2E).
195
196 To ensure that entospletinib did not have deleterious effects on *L. amazonensis*
197 amastigotes, we incubated axenic amastigotes with entospletinib for 72 h and assessed
198 parasite survival with alamarBlue® (Ullah *et al.*, 2020). Entospletinib's EC_{50} against
199 axenic amastigotes in this assay was > 20 μM. The CC_{50} for RAW 264.7 cells over 72 h
200 was 3.3 ± 1.2 μM (3 biological replicates performed; see representative log concentration
201 response curves in Fig. S1D). These studies indicated that entospletinib did not kill either
202 *Leishmania* parasites or host cells over the time period and concentrations studied in
203 these uptake assays. To test whether entospletinib affected the intracellular survival of *L.*
204 *amazonensis* amastigotes post-internalization, we engineered *L. amazonensis* parasites
205 that expressed mNeonGreen (see methods) and allowed these amastigotes to be taken
206 up by RAW 264.7 cells. 24 h later, we added DMSO or 0.5 μM entospletinib (a
207 concentration where effects on host cells were minimal) for 72 h. We found no apparent
208 defects in the ability of amastigotes to survive within 0.5 μM entospletinib-treated RAW
209 264.7 cells compared to DMSO-treated RAW 264.7 cells over 72 h (Fig. S1E).
210

211 We next explored the mechanism by which entospletinib affected the
212 internalization of *Leishmania* parasites. First, we determined that extending uptake over
213 longer periods (up to 3 h) did not enable treated RAW 264.7 cells to overcome
214 entospletinib-mediated defects in *Leishmania* internalization (promastigotes shown in Fig.
215 S1F; amastigotes shown in Fig. S1G). To more specifically characterize the effects of
216 entospletinib on phagocytic cup formation, we performed an uptake assay with
217 amastigotes as described above, then incubated samples with far-red phalloidin. As has
218 previously been described for SYK inhibition, we found using confocal microscopy that
219 phagocytic cups seemed unable to close in entospletinib-treated RAW 264.7 cells (Fig.
220 S2), particularly since there were no differences in the numbers of cups seen between
221 DMSO and entospletinib-treated Mϕs (Fig. S3A). In addition, actin staining in phagocytic
222 cups was brighter on-average in entospletinib-treated compared to DMSO-treated RAW
223 264.7 cells (Fig. S3B), suggesting a direct effect on actin polymerization during
224 phagocytic cup formation.
225

226 **Host cell SYK is required for efficient phagocytosis and *Leishmania* uptake by Mϕs**

227 Given that kinase inhibitors can potentially have off-target effects, and could also
228 be acting upon either parasites or host cells, we next specifically tested the role of host
229 cell SYK during *Leishmania* uptake by Mϕs. Using BMDMs isolated from mice lacking
230 SYK in the monocyte lineage (*Syk*$^{flox/flox}$ LysM Cre+, abbreviated as *Syk*$^{-/-}$ when
231 discussing isolated BMDM), we found that *Syk*$^{-/-}$ BMDM demonstrated decreases in
232 promastigote (Fig. 3A, B) and amastigote uptake (Fig. 3B), by 38 ± 5% and 73 ± 3%,
233 respectively. The total number of promastigotes or amastigotes bound to BMDM was not

234 affected (Fig. 3C). *Syk*$^{-/-}$ BMDM also exhibited defects in C3bi and IgG-mediated
235 phagocytosis of coated beads (which were decreased by 43 ± 3% and 65 ± 10%,
236 respectively; Fig. 3D, E).
237
238 ***Leishmania* stimulates SFK-Arg-SYK signaling in Mϕs to stimulate uptake**
239 We next explored whether *L. amazonensis* employs signaling by the adhesion
240 molecule PSGL1 (CD162) to facilitate uptake. PSGL-1 has not been shown to be a
241 receptor for *Leishmania* uptake, but it is known to activate SYK signaling via interactions
242 with FcR (Zarbock *et al.*, 2008). We studied both of these possibilities using an antibody
243 known to block PSGL-1 signaling (Zanardo *et al.*, 2004), which should also prevent
244 *Leishmania* from directly interacting with PSGL-1. We found that this antibody did not
245 affect *Leishmania* internalization (Fig. S3C). In addition, entospletinib still prevented
246 *Leishmania* uptake when added alongside the antibody (Fig. S3D).
247
248 SFK and Abl family kinases have been shown to partly signal through SYK in
249 previous studies (Greuber and Pendergast, 2012). We have shown that Hck/Fgr/Lyn
250 specifically activates Abl2/Arg to facilitate amastigote uptake by Mϕs (Wetzel *et al.*, 2012;
251 Wetzel *et al.*, 2016). SFK are not required for C3bi-mediated phagocytosis in our system
252 (Wetzel *et al.*, 2016). Abl1, but not SFK or Arg, is required for efficient promastigote
253 uptake (Wetzel *et al.*, 2012; Wetzel *et al.*, 2016). Therefore, we hypothesized that an FcR-
254 SFK-Arg-SYK signaling pathway would be required for amastigote uptake, and a CR3-
255 Abl-SYK signaling pathway would be responsible for promastigote uptake. To test this
256 hypothesis, we performed experiments using combinations of kinase inhibitors and

257 activators (Mohamed *et al.*, 2022). Treating *Syk*$^{-/-}$ BMDM with imatinib to inhibit Abl family
258 kinases did not further decrease *Leishmania* promastigote uptake, and similarly, treating
259 *Syk*$^{-/-}$ BMDM with SU6656 to inhibit SFK or imatinib to inhibit Abl family kinases did not
260 further diminish *Leishmania* amastigote uptake (Fig. 4A). Adding entospletinib neither
261 further decreased promastigote uptake by BMDM lacking Abl (*Abl*$^{flox/flox}$ LysM Cre+
262 BMDM; abbreviated in figure as *Abl*$^{-/-}$) nor further impaired amastigote uptake by BMDM
263 lacking Hck, Fgr, and Lyn (*HFL*$^{-/-}$ BMDM) or Arg (*Arg*$^{-/-}$ BMDM) kinases (Fig. 4B). In
264 addition, the Arg/Abl activator DPH did not rescue the uptake of *Leishmania*
265 promastigotes or amastigotes by *Syk*$^{-/-}$ BMDM (Fig. 4C).
266
267 We then investigated whether SFK and Abl family kinases were essential for SYK
268 activation during amastigote uptake. We chose to focus on amastigotes as the more
269 biologically relevant life cycle stage in human infection. We allowed Mϕs to begin
270 internalizing amastigotes and performed immunoblots for phosphorylated SYK (pSYK),
271 normalized to total SYK levels. We found that pSYK levels were decreased after inhibition
272 of SFK (using SU6656) or Abl family kinases (using imatinib), while activating Abl family
273 kinases using DPH increased Syk phosphorylation (Fig. 5A, B; see Fig. S4 for full Western
274 blot images and additional examples). Previously, we have shown that SFK and Abl family
275 kinases are required for effective phosphorylation of their substrate CrkII (*i.e.*, pCrk)
276 during amastigote uptake by Mϕs (Wetzel *et al.*, 2012; Wetzel *et al.*, 2016). To determine
277 whether SYK was required for this phosphorylation event, we probed for pCrk induction
278 upon amastigote uptake by entospletinib-treated Mϕs. We found lower levels of pCrk in

279 entospletinib-treated Mϕs undergoing amastigote uptake when compared to DMSO
280 controls (Fig. 5C, D; Fig. S4).
281
282 **SYK inhibition reduces lesion size and parasite burden in cutaneous leishmaniasis**
283 Knowing that SYK was required for efficient uptake of *Leishmania* by Mϕs, we
284 investigated whether its activity was required for the manifestations of cutaneous
285 leishmaniasis in mice. We infected *Syk*$^{flox/flox}$ LysM Cre+ mice and WT mice in the right
286 hind foot with *L. amazonensis* promastigotes and monitored lesion size over time. We
287 found that *Syk*$^{flox/flox}$ LysM Cre+ mice developed smaller lesions than WT mice (Fig. 6A),
288 suggesting that SYK activity is necessary for maximal pathogenesis of cutaneous
289 leishmaniasis in the mouse model.
290
291 The smaller lesions seen in *Syk*$^{flox/flox}$ LysM Cre+ mice potentially could be the
292 result of differences in their immunological responses to infection. As a simplified
293 paradigm, Th1 responses to leishmaniasis are typically protective, and Th2 responses
294 are generally deleterious to the infected host (Jones *et al.*, 1998). Therefore, we isolated
295 draining lymph nodes from infected WT and *Syk*$^{flox/flox}$ LysM Cre+ mice and assayed
296 cytokine secretion after stimulation with parasite lysates compared to Concanavalin A
297 (Con A) stimulation (a positive control) or no stimulation (a negative control). Overall, we
298 found limited differences between these two categories of mice (Table 1; Fig. S5A-E),
299 with the exception of IL1β induction, which SYK is known to facilitate (Callaway *et al.*,
300 2015). However, decreases in IL1β have been associated with worsening lesions (Lima-

301 Junior *et al.*, 2013). We also did not see any changes in the overall ratio of Th1 vs Th2
302 cytokine release (Table S1).
303
304 Based on our data that SYK activity is required for *Leishmania* uptake by
305 macrophages, we hypothesized that there would be fewer parasites contained within
306 lesions of infected *Syk*$^{flox/flox}$ LysM Cre+ mice. Indeed, at experimental termination (wk
307 18), we found that lesions in *Syk*$^{flox/flox}$ LysM Cre+ mice contained fewer parasites than
308 WT mice (Fig. 6B).
309
310 Next, we tested whether inhibition of SYK with entospletinib decreased lesion size
311 and parasite burden. We found that entospletinib-treated mice developed smaller lesions
312 than diluent/DMSO-treated mice over time (Fig. 6C). There were minimal effects on
313 cytokine secretion when draining lymph nodes isolated from DMSO-treated infected mice
314 were treated with entospletinib during cell culture (Table 2; Fig. S5F-I). The lone
315 statistically significant result was an increase in IL-13 in some stimulated entospletinib-
316 treated samples. Finally, we demonstrated that lesions in entospletinib-treated mice
317 contained significantly fewer parasites than DMSO-treated mice at the termination of the
318 experiment (wk 20, Fig. 6D).
319
320 In summary, we have demonstrated that SFK and Abl family kinases activate SYK
321 to facilitate phagocytosis, the uptake of *Leishmania* by Mϕs, and the disease
322 manifestations seen in experimental cutaneous leishmaniasis. In combination with our
323 previous results (Wetzel *et al.*, 2012; Wetzel *et al.*, 2016), these findings suggest that

324 preventing parasite uptake by host cells using kinase inhibitors could be a valid strategy

325 for designing novel antileishmanial therapies.

326

327 **DISCUSSION**

328 We have shown previously that host SFK and Abl family kinases promote
329 *Leishmania* uptake by Mϕs (Wetzel *et al.*, 2012; Wetzel *et al.*, 2016). Our results here
330 demonstrate that SYK also is necessary for maximal *Leishmania* promastigote and
331 amastigote uptake by Mϕs. Activation of SYK by SFK and Abl family kinases in Mϕs
332 facilitates *Leishmania* internalization. Finally, mice lacking SYK in monocytes or treated
333 with the SYK kinase inhibitor entospletinib exhibit significantly reduced lesion severity and
334 parasite burden when infected with *Leishmania amazonensis*. Our data lead us to
335 propose a relationship between FcR signaling, SFKs, Arg, and SYK during *Leishmania*
336 amastigote uptake. Upon FcR ligation by amastigotes, Hck, Fgr, and Lyn are activated.
337 These SFKs phosphorylate and activate Arg kinase, which phosphorylates and activates
338 SYK, which leads to activation of CrkII, actin polymerization at the site of cell entry and
339 formation/closure of the phagocytic cup (Fig. 6E).

340

341 Engagement of FcR stimulates downstream responses important for host
342 immunity and receptor-mediated phagocytosis. Our results demonstrate that FcR-
343 mediated signals permitting *Leishmania* amastigote uptake are relayed to SYK. SYK
344 previously was shown to facilitate phagocytosis after opsonized particles bind FcR on
345 phagocytic cells (Crowley *et al.*, 1997). Reductions in IgG-mediated phagocytosis by
346 *Syk*$^{-/-}$ BMDM were previously described to be secondary to defects in phagocytic cup
347 formation and closure, rather than defects in Mϕ activation (Crowley *et al.*, 1997), which
348 is supported by our data. The effects of the novel SYK inhibitor, entospletinib, on
349 phagocytosis had not been explored to date. We find that fewer IgG-coated beads or

350 *Leishmania* amastigotes are internalized by entospletinib-treated Mϕ or Mϕ deficient in
351 SYK. Neither condition changes the numbers of beads or parasites bound to Mϕ. The role
352 of SYK in C3bi-mediated phagocytosis has been somewhat controversial (Kiefer *et al.*,
353 1998; Tohyama and Yamamura, 2006; Walbaum *et al.*, 2021). Our evidence supports
354 SYK as a major contributor to efficient C3bi-mediated phagocytosis. Importantly, we also
355 establish that SYK promotes the uptake of *Leishmania* promastigotes.
356
357 Multiple signaling pathways are regulated by SYK during phagocytosis, including
358 linker for activation of T cells (LAT, (Balagopalan *et al.*, 2015)), phospholipase
359 Cγ (PLCγ , (Karimi *et al.*, 1999)), and phosphatidylinositol 3-kinase (PI3-K, (Yamamori *et*
360 *al.*, 2000)). In addition, PI3-K signaling has been specifically implicated in *Leishmania*
361 uptake by phagocytic cells (Cummings *et al.*, 2012). In combination with previous studies,
362 our experiments indicate that the specific signaling events necessary for FcR-mediated
363 *Leishmania* amastigote internalization are initiated by the activation of SFK, which
364 proceed to phosphorylate Arg kinase, which in turn phosphorylates SYK. Our data with
365 entospletinib suggest that actin polymerization within phagocytic cups is increased,
366 consistent with our prior findings using Mϕ lacking Abl family kinases (Wetzel *et al.*, 2012).
367 The pSYK antibody used here specifically recognizes phosphorylation on Tyr525/526,
368 which are SYK autophosphorylation sites that are necessary for maximal activity. Based
369 on our data, we presume that Abl family kinases are modulating the phosphorylation of
370 these two residues during amastigote uptake. However, our data do not rule out the
371 possibility that other sites on SYK may also be phosphorylated. The link between Abl
372 family kinases and SYK is likely to be direct, as previous studies have demonstrated that

373 purified Arg kinase phosphorylates SYK *in vitro* (Bonnerot *et al.*, 1998; Greuber and
374 Pendergast, 2012; Parsa *et al.*, 2008). Similarly, SFK have been shown to phosphorylate
375 Arg kinase *in vitro* (Mader *et al.*, 2011; Plattner *et al.*, 2004; Tanis *et al.*, 2003). We
376 explored whether the extracellular domains of PSGL-1, which is known to activate SYK
377 signaling via interactions with FcR (Zarbock *et al.*, 2008), also participated in this signaling
378 cascade, but were unable to find evidence that this alternate receptor was relevant during
379 *Leishmania* uptake. However, the methods we used would not address the possibility that
380 signaling occurs through the intracellular domains of PSGL-1; additional experiments will
381 be conducted for this purpose. In addition, this study, in combination with our prior work
382 (Wetzel *et al.*, 2012; Wetzel *et al.*, 2016) demonstrates that activation of SFK, Abl family
383 kinases and SYK after FcR binding results in CrkII activation during the uptake of
384 *Leishmania* parasites. A number of other downstream mediators of SYK signaling have
385 been published (Mocsai *et al.*, 2010). Our future studies will directly test whether these
386 mediators, or other kinases previously thought to facilitate phagocytosis or internalization
387 of other pathogens, also participate in the uptake of *Leishmania*.
388
389 Because *Leishmania* parasites that remain extracellular within a mammalian host
390 are thought to either die or be killed by the host immune system, we tested whether SYK
391 deficiency would restrict disease manifestations in a mouse model of cutaneous
392 leishmaniasis. Our studies indicate that *Leishmania* survival and pathogenesis in mice
393 depends on SFK (Wetzel *et al.*, 2016), Abl/Arg (Wetzel *et al.*, 2012; Wetzel *et al.*, 2016),
394 and now SYK. We believe that the smaller lesions seen in SYK-deficient mice primarily
395 occur due to the deficits we identified in parasite internalization by phagocytes. Consistent

396 with this hypothesis, there are fewer parasites within the lesions of SYK-deficient mice or
397 mice treated with entospletinib. Since our hypothesis is difficult to test directly, our
398 conclusions in part stem from eliminating other possibilities. For example, we found that
399 entospletinib did not kill *Leishmania* parasites directly, and we saw no defects in parasite
400 survival within entospletinib-treated Mϕs.
401
402 Furthermore, we assessed whether the reductions in lesion size observed in SYK-
403 deficient mice could be due to variations in the host immune response to leishmaniasis
404 compared to control mice. For example, SYK deficiency is known to affect B and T cell
405 development in mice and immune cell adhesion (Mocsai *et al.*, 2010), which might
406 adversely affect the host's ability to control infections. However, our results suggest that
407 such defects play a more limited role in our experimental system. The overall innate
408 immune response to leishmaniasis is complex and dependent upon the infecting parasite
409 species and the mouse strain used. In general, Th1 responses lead to lesion healing and
410 Th2 responses result in lesion worsening (Jones *et al.*, 1998). Our profiling of cytokines
411 secreted by isolated lymph nodes after infection revealed no significant differences in Th1
412 versus Th2 responses between SYK-deficient and control mice. Lymph nodes from
413 *Syk*$^{flox/flox}$ LysM Cre+ mice did exhibit defects in IL1-β secretion, which is known to be
414 partly dependent on SYK (Callaway *et al.*, 2015). However, we would expect that a
415 decrease in IL1-β would worsen lesions based on prior studies (Lima-Junior *et al.*, 2013).
416 Similarly, we did not see differences in secretion of cytokines from lymph nodes isolated
417 from infected mice that were incubated in entospletinib, save for an increase in IL-13 in
418 some stimulated entospletinib-treated samples, which also should not mediate lesion

419 healing (Jones *et al.*, 1998). Therefore, we saw no differences in the immune response
420 to leishmaniasis from our cytokine profiling that would explain the decreased lesion size
421 in mice deficient in SYK or treated with entospletinib. However, further studies are needed
422 to fully delineate changes in the immunological response to SYK inhibition in experimental
423 murine leishmaniasis.
424
425 **CONCLUSION**
426 In summary, our studies demonstrate that SYK is required for maximal *Leishmania*
427 uptake by Mϕs and disease in mice. Our future work will continue to trace the signaling
428 pathways necessary for internalization of this parasite by Mϕ, with an eye towards using
429 inhibitors of these pathways as treatment for leishmaniasis. A host-targeted therapeutic
430 strategy is likely to be less susceptible to the development of resistance. While our studies
431 have thus far focused on *Leishmania*, our findings likely are more broadly applicable, as
432 other intracellular pathogens also utilize and activate SYK to facilitate receptor-mediated
433 uptake. For example, overexpression of membrane-targeted SYK in cells treated with Abl
434 kinase inhibitors partially rescues the impairment in phagocytosis of *Francisella tularensis*
435 (Parsa *et al.*, 2008). Thus, there is potential to harness host kinases such as SYK as
436 targets for a broad-spectrum antimicrobial agent against intracellular pathogens.
437

438 **MATERIALS AND METHODS**

439 **Mice**

440 The UT Southwestern Institutional Animal Care and Use Committee approved all animal
441 protocols. *Syk*$^{flox/flox}$ *LysM Cre*+ and *Syk*$^{flox/flox}$ *LysM Cre*- littermates were generated by
442 crossing *LysM Cre*+ mice to *Syk*$^{flox/+}$ mice (all on a C57BL/6J background, which along
443 with WT C57BL/6J mice, had been purchased from Jackson Labs (Bar Harbor, ME)).
444 *Hck*$^{-/-}$ *Fgr*$^{-/-}$ *Lyn*$^{-/-}$, *Arg*$^{-/-}$ and *Abl*$^{flox/flox}$ *LysM Cre*+ mice were generated as described
445 previously (Wetzel *et al.*, 2012). For all experiments, WT littermates were paired with the
446 kinase mutant under study to limit any effects from variation in genetic backgrounds.

447

448 **Mammalian cell culture**

449 RAW 264.7 cells (obtained from ATCC, Manassas, VA) were incubated in Dulbecco's
450 modified Eagle's medium (DMEM) (ThermoFisher, Waltham, MA) plus 10% heat-
451 inactivated fetal bovine serum (FBS, Gemini). Bone marrow-derived primary Mϕs
452 (BMDM) were harvested from tibias of *Syk*$^{flox/flox}$ *LysM Cre*+, *Syk*$^{flox/flox}$ *LysM Cre*-, *Hck*$^{-/-}$
453 *Fgr*$^{-/-}$ *Lyn*$^{-/-}$, WT, *Arg*$^{-/-}$, and/or *Abl*$^{flox/flox}$ *LysM Cre*+ mice and confirmed as described
454 (Wetzel *et al.*, 2012). All cells were screened for *Mycoplasma* contamination (Wetzel *et*
455 *al.*, 2016).

456

457 ***Leishmania* culture**

458 *L. amazonensis* strain IFLA/BR/67/PH8 promastigotes (obtained from Norma W.
459 Andrews, University of Maryland, College Park, MD) were grown in Schneider's
460 Drosophila medium (Sigma, St. Louis, MO) with 15% heat-inactivated FBS and 10 μg/ml

461 gentamicin (Sigma) (Wetzel *et al.*, 2012). 7 day old cultures were used for uptake
462 experiments to maximize yield of infective metacyclic promastigotes. *L. amazonensis*
463 strain IFLA/BR/67/PH8 amastigotes were grown axenically (outside of mammalian cells)
464 in supplemented Schneider's media at pH 5 as described (Hodgkinson *et al.*, 1996). All
465 parasites were serially passaged through mice so that virulence would be maintained.
466

467 **Transgenic *Leishmania* strains**

468 For intracellular survival assays, *L. amazonensis* expressing a bright monomeric
469 green fluorescent protein, mNeonGreen, was used. mNeonGreen was cloned into the
470 pLEXSY.hyg2 (Jenabioscience, Jena, Germany) expression vector with a hygromycin
471 resistance marker, as previously described (Ullah *et al.*, 2020). pLEXSY.hyg2 containing
472 mNeonGreen gene (pLEXSY.hyg2-mNeonGreen) was transfected into *L.*
473 *amazonensis* promastigotes using the Human T-Cell Nucleofector kit and the Amaxa
474 Nucleofector electroporator (program U-033, Lonza, Basel, Switzerland), for integration
475 into the 18S rRNA locus within the nuclear DNA. Following transfections, promastigotes
476 were allowed to grow for 24 h at 26 °C, then selected with 100 µg/mL hygromycin in
477 Schneider's Drosophila medium. Clones were isolated via limiting dilution, and the
478 cultures were subsequently maintained in Schneider's Drosophila medium supplemented
479 with 100 µg/mL hygromycin. To maintain virulence, *L. amazonensis*-mNeonGreen
480 expressing parasites were passaged regularly in C57BL/6 mice, as described previously
481 (Wetzel *et al.*, 2016).
482

483 **Phagocytosis assays**

484 BMDM and RAW 264.7 cells were plated at > 50% confluence and starved overnight in
485 macrophage-colony stimulating factor (M-CSF)-starved or serum-free media. For drug
486 experiments, except where indicated, compounds were obtained from LC Laboratories
487 (Woburn, MA). Mϕ were incubated in 3.3 μM imatinib, 1 μM SU6656, 1 μM entospletinib,
488 or 0.1% DMSO (Sigma) for 2 h. For C3bi-coated bead internalization only, Mϕ were also
489 pre-activated with PMA (Sigma) for 1 h. As described (Wetzel *et al.*, 2012; Wetzel *et al.*,
490 2016), 2 μm latex green beads were incubated with human IgM (I-8260, Sigma), then in
491 rabbit anti-human IgM (Sigma 270A, IgG-coated beads) or fresh mouse serum (C3bi-
492 coated beads). 10 beads/ Mϕ were added to Mϕ for 30 m at 37 °C. To distinguish internal
493 from external beads, samples were fixed in 3% formaldehyde for 15 m, blocked in 2%
494 BSA (no permeabilization) (Wetzel *et al.*, 2004; Wetzel *et al.*, 2003; Wetzel *et al.*, 2005),
495 incubated in rabbit-anti human IgM and Hoescht 33258 (Sigma), and then incubated in
496 Alexa-Fluor-564-conjugated goat anti-rabbit IgG. Samples were visualized using a
497 Cytation 5 imager (BioTek, Santa Clara, CA) and analyzed by an observer blinded to
498 condition. Representative images for beads were collected on the Cytation 5 at 40X and
499 processed linearly in Adobe Photoshop (version 13.0.6) (Ullah *et al.*, 2020). The
500 phagocytic index (PI) was calculated as the number of beads internalized per 100 Mϕ,
501 and experimental samples were normalized to controls. The total number of beads per
502 100 Mϕ was also calculated, with experimental samples were normalized to controls. At
503 least 100 Mϕ and 100 beads were counted from multiple imaged fields per condition. All
504 experiments had at least 3 biological replicates performed, and means were calculated.
505 Each biological replicate was then normalized so that the control was set to 100% for
506 each experiment. The experimental category shown represents a percentage of this

507 control value with standard errors. A one-sample *t*-test was used for statistical analysis of
508 these results (Wetzel *et al.*, 2012; Wetzel *et al.*, 2016).
509
510 ***Leishmania* uptake assays**
511 RAW 264.7 cells or BMDMs were treated with DMSO/PMA/inhibitors as above. To allow
512 C3bi opsonization, we incubated metacyclic promastigotes in murine serum for 1 h. To
513 allow IgG opsonization, we incubated amastigotes with anti-P8 primary IgG1 antibody
514 (Pan and McMahon-Pratt, 1988) for 1 h. Opsonized parasites were incubated with Mϕ at
515 10:1 promastigotes per Mϕ or 2:1 amastigotes per Mϕ (Wetzel *et al.*, 2012; Wetzel *et al.*,
516 2016). Samples were fixed with 3% formaldehyde, blocked in 2% BSA in PBS, incubated
517 in mouse anti-gp46 antibody (promastigotes) or mouse anti-P8 antibody (both supplied
518 by Diane McMahon-Pratt), then incubated in Alexa-Fluor-568 goat-anti-mouse secondary
519 antibody (A10037, ThermoFisher) (Wetzel *et al.*, 2012). After permeabilization, parasites
520 were incubated in their original primary antibody, then Alexa-Fluor-488 donkey anti-
521 mouse secondary antibody (A21202, ThermoFisher) and Hoescht 33258 (Sigma).
522 Visualization, analysis, and statistics were performed as described above for bead
523 phagocytic assays (Wetzel *et al.*, 2012; Wetzel *et al.*, 2016). Representative images for
524 parasites were collected on a Zeiss LSM 880 inverted confocal Airyscan microscope at
525 40X (Ullah *et al.*, 2020). Shown are maximal intensity projections constructed from full Z-
526 thickness stacks through parasites/Mϕ using Image J (1.52a, http://imagej.nih.gov/ij) and
527 processed linearly in Adobe Photoshop (version 13.0.6) (Ullah *et al.*, 2020).
528

529 For PSGL-1 experiments, amastigotes were incubated with anti-P8 primary IgG1 antibody
530 (Pan and McMahon-Pratt, 1988) for 1 h. RAW 264.7 cells were pre-treated with anti-
531 mouse CD162 (PSGL-1) monoclonal antibody (4RA10; 12-1621-80, ThermoFisher),
532 entospletinib, both, or equal amounts of vehicle (DMSO) for 1 hr. Antibody was employed
533 at 1:2500, 1:1000, 1:500, 1:250, and 1:100, and entospletinib was applied at 1 uM.
534 Opsonized parasites were incubated with RAW 264.7 cells at 10:1, respectively. Samples
535 were fixed with 4% formaldehyde, blocked in 5% BSA/PBS, incubated in mouse anti-P8
536 antibody, then incubated in Alexa-Fluor-568 goat-anti-mouse secondary antibody
537 (A10037, ThermoFisher) (Wetzel et al., 2012). After permeabilization with 0.1% Triton-
538 X114, parasites were incubated in their original primary antibody, then Alexa-Fluor-488
539 donkey anti-mouse secondary antibody (A21202, ThermoFisher) and Hoescht 33258
540 (Sigma). Visualization was performed on an INCell Analyzer 6000™ (GE Healthcare, Inc.)
541 microscope at 40x in the UTSW High Throughput Screening Core facility. For Fig. S3C,
542 images were processed through a CellProfiler pipeline (https://cellprofiler.org). 3-6
543 technical replicates were performed for each condition and 3 separate biological
544 replicates were combined to provide the data shown. Statistics were performed as above
545 for phagocytic assays (Wetzel et al., 2012; Wetzel et al., 2016). Fig. S3D was analyzed
546 as indicated under the “Phagocytosis assays” and “Leishmania uptake assays” headings.

547

548 **Viability assays**

549 *L. amazonensis* promastigotes, axenic amastigotes, and RAW 264.7 cells were cultured
550 as above, added to 96 well plates containing dilution series of relevant compounds, and
551 incubated for 72 h before measuring viability using alamarBlue® (10%, ThermoFisher)

552 (Ullah *et al.*, 2020). Plates were read at 6 h with a BioTek Synergy H1 plate reader (530
553 nm excitation, 570 nm emission) (Ullah *et al.*, 2020). To assess for parasite survival, 10
554 *L. amazonensis* promastigotes/Mϕ were added to G-CSF starved WT BMDMs and
555 incubated for 4 h. After 5 washes with PBS, DMSO or 1 μm entospletinib was added in
556 media with G-CSF. Samples were analyzed after 72 h by microscopy using the Cytation
557 5 imager, and total numbers of amastigotes/Mϕ were calculated by a blinded observer
558 using the methods described above for phagocytosis assays.
559

560 **Immunoblotting**

561 To measure phosphorylation of SYK or CrkII, RAW 264.7 cells were incubated overnight
562 in serum-free media with experiments performed at ~70% confluence. To initiate
563 experiments, RAW cells were pre-incubated in 3.3 μM SU6656, 3.3 μM imatinib, 1 μM
564 entospletinib, 50 nM DPH or DMSO for 2 h. IgG-opsonized amastigotes were added to
565 adherent starved RAW 264.7 cells (at a ratio of 20:1) for 30 m (Pan and McMahon-Pratt,
566 1988). Cells were lysed with Pierce Radioimmunoprecipitation (RIPA) buffer (cat. no.
567 89901, Thermo Scientific, Rockford, IL) with protease and phosphatase inhibitors, and
568 protein concentrations were assessed using bicinchoninic acid (BCA) (cat. no. 23225,
569 Thermo Scientific). For representative images, equivalent protein amounts were loaded
570 on 10% SDS-PAGE gels, transferred to nitrocellulose membranes, and probed with
571 antibodies against phosphorylated Syk (pSyk) (Tyr525/526, cat. no. 2710S, Cell
572 Signaling, Danvers, MA) at 1:500, or Syk (cat. no. 2712S, Cell Signaling) at 1:500.
573 Immunoblotting with rabbit GAPDH (cat. no. 2118L, Cell Signaling) at 1:1000 was used
574 as a loading control. For analysis, relative amounts of pSyk or pCrkII were compared with

575 Image J analysis software and were normalized to Syk or CrkII (membranes were stripped
576 of pSyk or pCrk and reprobed for Syk or Crk). Imaging was performed by using a
577 phosphorimager (ImageQuant LAS 4000, GE, Boston, MA). Each experiment was
578 performed 4 times. Two-way ANOVA was used to determine statistical significance.
579
580 **Murine infections**
581 8 week old female C57BL/6 mice were infected in the dorsal side of the right hind foot
582 with 1 X 10^6 metacyclic promastigotes (isolated via Percoll gradient, Sigma) per mouse;
583 10 mice were used per experimental condition. All animals surviving until termination were
584 included in analysis. For entospletinib-treated mice, 3 experiments were conducted. Mice
585 were provided 100 mg/kg/d of entospletinib or the diluent (0.1 % DMSO) in their drinking
586 water at pH 5.5, starting 4 days prior to the experiment and continuing through termination
587 (Wetzel *et al.*, 2016). For *Syk*$^{flox/flox}$ *LysM Cre*+ mice, 3 independent experiments were
588 conducted. Lesion size was measured every other week with calipers by a condition-
589 blinded investigator, and infected/uninfected foot thickness ratios were calculated and
590 compared to time of infection by ANOVA. The number of parasites in lesions were
591 determined at the time of experiment termination (between 18 and 20 wks post-infection)
592 (Soong *et al.*, 1997).
593
594 Lymph nodes from infected mice were harvested for cytokine profiling as described
595 (Wetzel *et al.*, 2012; Wetzel *et al.*, 2016). In brief, cells from lymph nodes were plated and
596 stimulated with varying concentrations of promastigote lysates (high stimulation = 2.5 X
597 10^6 parasites; low = 5 X 10^5 parasites) or concanamycin A (CON A) (5 μg/ml, Sigma);

598 supernatants were harvested at 72 h. A negative (unstimulated control) was employed to
599 ensure that cytokines released were secondary to stimulation, and levels of all measured
600 cytokines were found to be negligible compared to background. Levels of IL-1β, IL-4, IFN-
601 γ, IL-10, IL-13, and IL-17 were assessed by ELISA and compared to background
602 (unstimulated) levels.
603

604 **Acknowledgements**

605 We thank the parasitology group at UT Southwestern (Drs. James J. Collins,
606 Margaret A. Phillips, and Michael L. Reese), as well as members of the UT Southwestern
607 Departments of Biochemistry, Microbiology, Pharmacology, and Pediatrics for valuable
608 discussions and use of common equipment. Gina M. Aloisio, Lauren T. Callaghan, Ivan
609 Luu, Hanspeter Niederstrasser, T. Michael Oladugba, and Catherine L. Trice provided
610 expert technical assistance. Dr. Naomi S. Morrissette (UC Irvine) supplied helpful
611 comments on the manuscript, and Drs. Anthony J. Koleske and Diane McMahon-Pratt
612 (both from Yale University) offered valuable advice as this project was conceived.
613 Antileishmanial antibodies were donated by Dr. McMahon-Pratt. *Arg*$^{-/-}$, *Abl*$^{flox/flox}$, and *Arg*$^{-}$
614 $^{/-}$ *Abl*$^{flox/flox}$ mice were provided by Dr. Koleske. *Hck*$^{-/-}$ *Fgr*$^{-/-}$ *Lyn*$^{-/-}$ mice were provided by
615 Shaoguang Li. Confocal microscopy was performed in the UT Southwestern Live Cell
616 Imaging Facility.
617

618 **Competing interests**

619 The authors declare that they have no competing financial interests.
620

621 **Author contributions**

622 I.U., U.B., A.D., and D.M.W. designed and performed experiments, analyzed data,
623 and wrote the manuscript. R.M.K., F.T.H.K., E.T.M., L.M.B, E.L.R., and J.M.B. performed
624 experiments and analyzed data.

625

626 **Funding**

627 This work was supported by the National Institutes of Health (K08 AI103036 and R01
628 AI146349), a Children's Clinical Research Advisory Committee (CCRAC) Junior
629 Investigator Award, a CCRAC Early Investigator Award, grant I-2086 from the Welch
630 Foundation, and funds from the UT Southwestern Department of Pediatrics (all to
631 D.M.W.). In addition, U.B. was supported by a National Institutes of Health Supplement
632 To Promote Diversity in Health-Related Research (R01 AI146349-S1) and the Medical
633 Scientist Training Program at UT Southwestern (NIH T32GM008014). F.T.H.K. was a
634 member of the Green Fellows Program, which is generously supported by UT Dallas and
635 the Cecil and Ida Green Foundation.

636

637 **Data availability**

638 This manuscript was uploaded to Biorxiv as a preprint prior to publication
639 (BIORXIV/2022/513575). All data referenced in this manuscript is available upon
640 publication within the main body or supplementary data sections or on Biorxiv.

641

642 **REFERENCES**

643 Baker, N. *et al.* Systematic functional analysis of Leishmania protein kinases
644 identifies regulators of differentiation or survival. *Nat Commun*, **2021,** 12:1244.

645 Balagopalan, L. *et al.* The linker for activation of T cells (LAT) signaling hub: from
646 signaling complexes to microclusters. *J Biol Chem*, **2015,** 290:26422-9.

647 Bonnerot, C. *et al.* Syk protein tyrosine kinase regulates Fc receptor gamma-
648 chain-mediated transport to lysosomes. *EMBO J*, **1998,** 17:4606-16.

649 Bradley, W. D. and Koleske, A. J. Regulation of cell migration and
650 morphogenesis by Abl-family kinases: emerging mechanisms and physiological
651 contexts. *J Cell Sci*, **2009,** 122:3441-54.

652 Bradshaw, J. M. The Src, Syk, and Tec family kinases: distinct types of molecular
653 switches. *Cell Signal*, **2010,** 22:1175-84.

654 Callaway, J. B. *et al.* Spleen tyrosine kinase (Syk) mediates IL-1beta induction by
655 primary human monocytes during antibody-enhanced Dengue virus infection. *J Biol*
656 *Chem*, **2015,** 290:17306-20.

657 Crowley, M. T. *et al.* A critical role for Syk in signal transduction and
658 phagocytosis mediated by Fcgamma receptors on macrophages. *J Exp Med*, **1997,**
659 186:1027-39.

660 Cummings, H. E. *et al.* Critical role for phosphoinositide 3-kinase gamma in
661 parasite invasion and disease progression of cutaneous leishmaniasis. *Proc Natl Acad*
662 *Sci U S A*, **2012,** 109:1251-6.

663 Fitzer-Attas, C. J. *et al.* Fcgamma receptor-mediated phagocytosis in
664 macrophages lacking the Src family tyrosine kinases Hck, Fgr, and Lyn. *J Exp Med*,
665 **2000,** 191:669-82.
666 Furlong, M. T. *et al.* Identification of the major sites of autophosphorylation of the
667 murine protein-tyrosine kinase Syk. *Biochim Biophys Acta*, **1997,** 1355:177-90.
668 Greuber, E. K. and Pendergast, A. M. Abl family kinases regulate FcgammaR-
669 mediated phagocytosis in murine macrophages. *J Immunol*, **2012,** 189:5382-92.
670 Guy, R. A. and Belosevic, M. Comparison of receptors required for entry of
671 *Leishmania major* amastigotes into macrophages. *Infect Immun*, **1993,** 61:1553-8.
672 Hodgkinson, V. H. *et al. Leishmania amazonensis*: cultivation and
673 characterization of axenic amastigote-like organisms. *Exp Parasitol*, **1996,** 83:94-105.
674 Jones, D. E. *et al.* Host susceptibility factors to cutaneous leishmaniasis. *Front*
675 *Biosci*, **1998,** 3:D1171-80.
676 Karimi, K. *et al.* Protein kinase C and a calcium-independent phospholipase are
677 required for IgG-mediated phagocytosis by Mono-Mac-6 cells. *J Leukoc Biol*, **1999,**
678 65:854-62.
679 Kiefer, F. *et al.* The Syk protein tyrosine kinase is essential for Fcgamma
680 receptor signaling in macrophages and neutrophils. *Mol Cell Biol*, **1998,** 18:4209-20.
681 Kima, P. E. *et al.* Internalization of *Leishmania mexicana* complex amastigotes
682 via the Fc receptor is required to sustain infection in murine cutaneous leishmaniasis. *J*
683 *Exp Med*, **2000,** 191:1063-8.
684 Lima-Junior, D. S. *et al.* Inflammasome-derived IL-1beta production induces nitric
685 oxide-mediated resistance to Leishmania. *Nat Med*, **2013,** 19:909-15.

686 Lodge, R. and Descoteaux, A. Leishmania invasion and phagosome biogenesis.
687 *Subcell Biochem*, **2008,** 47:174-81.
688 Lowell, C. A. Src-family and Syk kinases in activating and inhibitory pathways in
689 innate immune cells: signaling cross talk. *Cold Spring Harb Perspect Biol*, **2011,** 3.
690 Mader, C. C. *et al.* An EGFR-Src-Arg-cortactin pathway mediates functional
691 maturation of invadopodia and breast cancer cell invasion. *Cancer Res*, **2011,** 71:1730-
692 41.
693 Mocsai, A. *et al.* The SYK tyrosine kinase: a crucial player in diverse biological
694 functions. *Nat Rev Immunol*, **2010,** 10:387-402.
695 Mohamed, M. F. *et al.* CrkII/Abl phosphorylation cascade is critical for NLRC4
696 inflammasome activity and is blocked by *Pseudomonas aeruginosa* ExoT. *Nat*
697 *Commun*, **2022,** 13:1295.
698 Mosser, D. M. *et al.* Leishmania promastigotes require opsonic complement to
699 bind to the human leukocyte integrin Mac-1 (CD11b/CD18). *J Cell Biol*, **1992,** 116:511-
700 20.
701 Pan, A. A. and McMahon-Pratt, D. Monoclonal antibodies specific for the
702 amastigote stage of *Leishmania pifanoi*. I. Characterization of antigens associated with
703 stage- and species-specific determinants. *J Immunol*, **1988,** 140:2406-14.
704 Parsa, K. V. *et al.* The tyrosine kinase Syk promotes phagocytosis of Francisella
705 through the activation of Erk. *Mol Immunol*, **2008,** 45:3012-21.
706 Parsons, M. *et al.* Comparative analysis of the kinomes of three pathogenic
707 trypanosomatids: *Leishmania major*, *Trypanosoma brucei* and *Trypanosoma cruzi*. *BMC*
708 *Genomics*, **2005,** 6:127.

709 Plattner, R. *et al.* Bidirectional signaling links the Abelson kinases to the platelet-
710 derived growth factor receptor. *Mol Cell Biol*, **2004,** 24:2573-83.
711 Puentes, S. M. *et al.* Complement binding by two developmental stages of
712 *Leishmania major* promastigotes varying in expression of a surface lipophosphoglycan.
713 *J Exp Med*, **1988,** 167:887-902.
714 Ramanathan, S. *et al.* Pharmacokinetics, pharmacodynamics, and safety of
715 entospletinib, a novel pSYK inhibitor, following single and multiple oral dosing in healthy
716 volunteers. *Clin Drug Investig*, **2017,** 37:195-205.
717 Russell, D. G. and Wright, S. D. Complement receptor type 3 (CR3) binds to an
718 Arg-Gly-Asp-containing region of the major surface glycoprotein, gp63, of Leishmania
719 promastigotes. *J Exp Med*, **1988,** 168:279-92.
720 Soong, L. *et al.* Role of CD4+ T cells in pathogenesis associated with *Leishmania*
721 *amazonensis* infection. *J Immunol*, **1997,** 158:5374-83.
722 Tanis, K. Q. *et al.* Two distinct phosphorylation pathways have additive effects on
723 Abl family kinase activation. *Mol Cell Biol*, **2003,** 23:3884-96.
724 Tohyama, Y. and Yamamura, H. Complement-mediated phagocytosis--the role of
725 Syk. *IUBMB Life*, **2006,** 58:304-8.
726 Ueno, N. and Wilson, M. E. Receptor-mediated phagocytosis of Leishmania:
727 implications for intracellular survival. *Trends Parasitol*, **2012,** 28:335-44.
728 Ullah, I. *et al.* An antiparasitic compound from the Medicines for Malaria Venture
729 Pathogen Box promotes *Leishmania* tubulin polymerization. *ACS Infect Dis*, **2020,**
730 6:2057-2072.

731 Walbaum, S. *et al.* Complement receptor 3 mediates both sinking phagocytosis
732 and phagocytic cup formation via distinct mechanisms. *J Biol Chem*, **2021,** 296:100256.
733 Walker, A. R. *et al.* Entospletinib in combination with induction chemotherapy in
734 previously untreated Acute Myeloid Leukemia: response and predictive significance of
735 HOXA9 and MEIS1 expression. *Clin Cancer Res*, **2020,** 26:5852-5859.
736 Wetzel, D. M. *et al.* Calcium-mediated protein secretion potentiates motility in
737 *Toxoplasma gondii*. *J Cell Sci*, **2004,** 117:5739-48.
738 Wetzel, D. M. *et al.* Actin filament polymerization regulates gliding motility by
739 apicomplexan parasites. *Mol Biol Cell*, **2003,** 14:396-406.
740 Wetzel, D. M. *et al.* The Abl and Arg kinases mediate distinct modes of
741 phagocytosis and are required for maximal *Leishmania* infection. *Molecular Cell*
742 *Biology*, **2012,** 32:3176-86.
743 Wetzel, D. M. and Phillips, M. A. Chapter 54: Chemotherapy of protozoal
744 infections. In *Goodman and Gilman's The Pharmacological Basis of Therapeutics*, (ed.
745 L. Brunton), New York, NY: McGraw-Hill Medical, 2018, pp. 987-999.
746 Wetzel, D. M. *et al.* The Src kinases Hck, Fgr, and Lyn activate Abl2/Arg to
747 facilitate IgG-mediated phagocytosis and *Leishmania* infection. *J Cell Sci*, **2016,**
748 129:3130-43.
749 Wetzel, D. M. *et al.* Gliding motility leads to active cellular invasion by
750 *Cryptosporidium parvum* sporozoites. *Infect Immun*, **2005,** 73:5379-87.
751 Wu, Y. *et al.* Role of Fc receptor gamma-chain in platelet glycoprotein Ib-
752 mediated signaling. *Blood*, **2001,** 97:3836-45.

753 Yamamori, T. *et al.* Roles of p38 MAPK, PKC and PI3-K in the signaling
754 pathways of NADPH oxidase activation and phagocytosis in bovine polymorphonuclear
755 leukocytes. *FEBS Lett*, **2000,** 467:253-8.
756 Zanardo, R. C. *et al.* A down-regulatable E-selectin ligand is functionally
757 important for PSGL-1-independent leukocyte-endothelial cell interactions. *Blood*, **2004,**
758 104:3766-73.
759 Zarbock, A. *et al.* PSGL-1 engagement by E-selectin signals through Src kinase
760 Fgr and ITAM adapters DAP12 and FcR gamma to induce slow leukocyte rolling. *J Exp*
761 *Med*, **2008,** 205:2339-47.
762
763

Figure 1

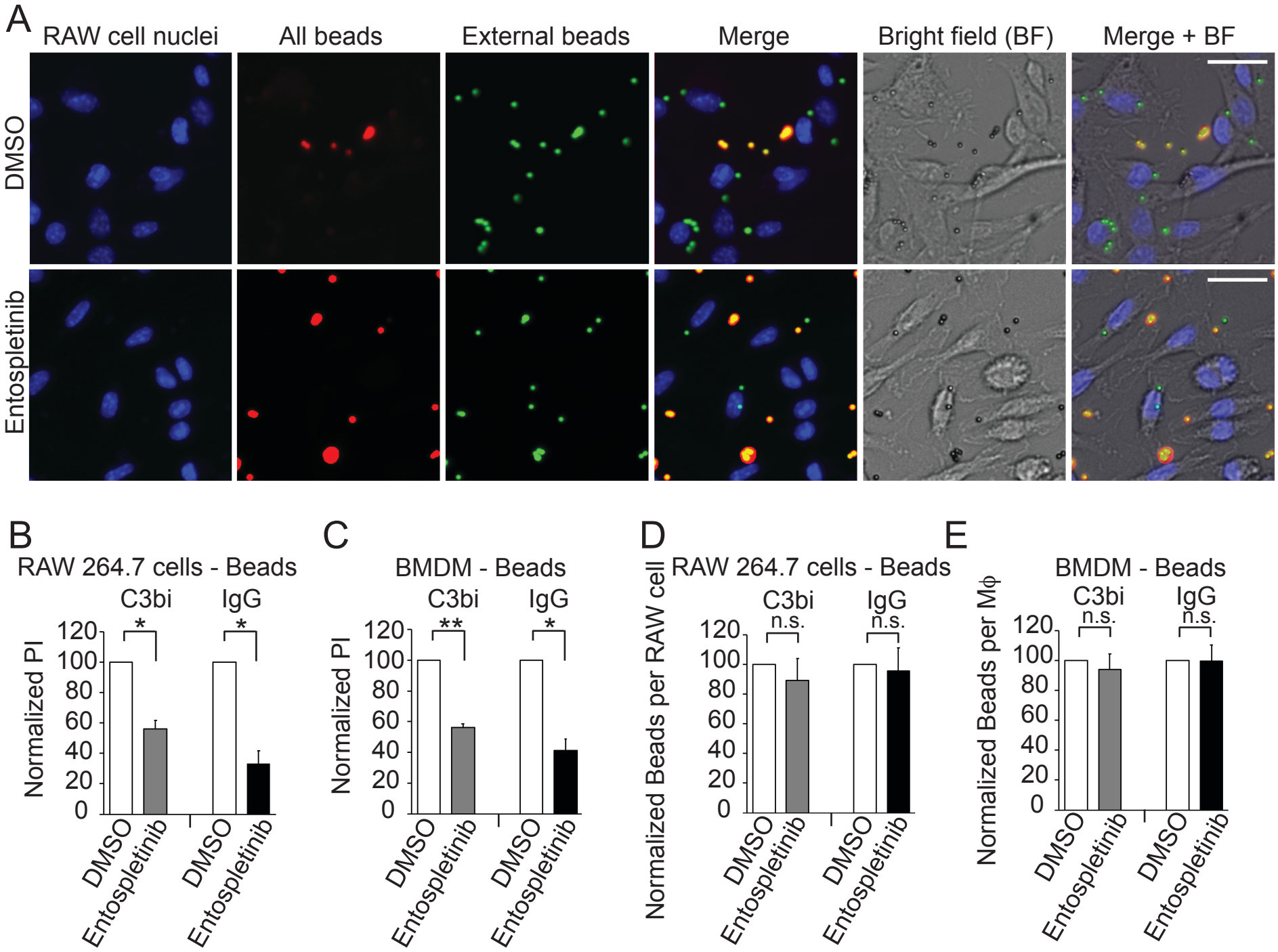
A
RAW cell nuclei
All beads
External beads
Merge
Bright field (BF)
Merge + BF
DMSO
Entospletinib
B
RAW 264.7 cells - Beads
C3bi
IgG
Normalized PI
120
100
80
60
40
20
0
*
*
DMSO
Entospletinib
DMSO
Entospletinib
C
BMDM - Beads
C3bi
IgG
Normalized PI
**
*
DMSO
Entospletinib
DMSO
Entospletinib
D
RAW 264.7 cells - Beads
C3bi
IgG
Normalized Beads per RAW cell
n.s.
n.s.
DMSO
Entospletinib
DMSO
Entospletinib
E
BMDM - Beads
C3bi
IgG
Normalized Beads per Mϕ
n.s.
n.s.
DMSO
Entospletinib
DMSO
Entospletinib

Figure 2

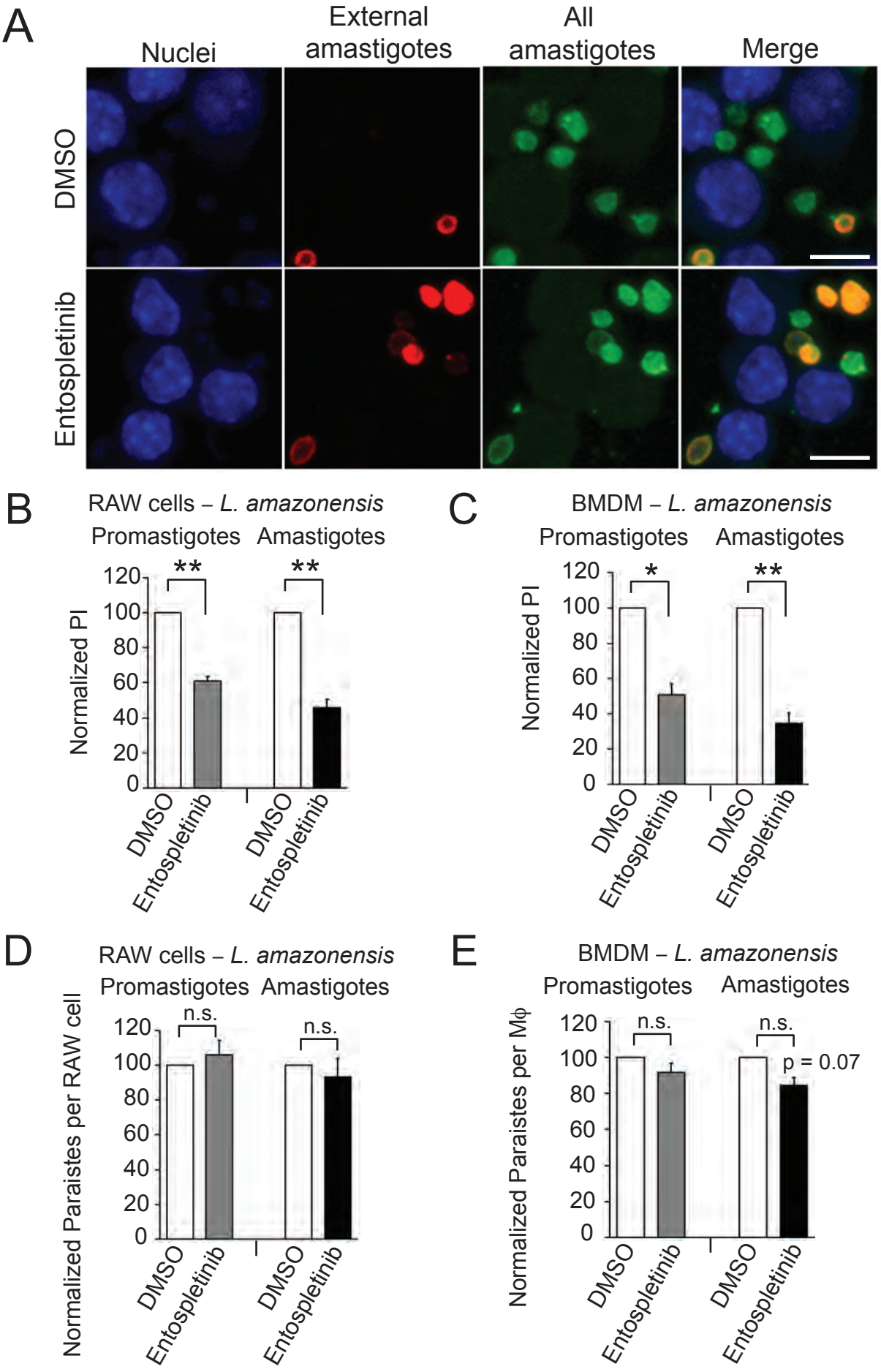
A
Nuclei
External amastigotes
All amastigotes
Merge
DMSO
Entospletinib
B
RAW cells – L. amazonensis
Promastigotes
Amastigotes
Normalized PI
120
100
80
60
40
20
0
**
**
DMSO
Entospletinib
DMSO
Entospletinib
C
BMDM – L. amazonensis
Promastigotes
Amastigotes
Normalized PI
*
**
DMSO
Entospletinib
DMSO
Entospletinib
D
RAW cells – L. amazonensis
Promastigotes
Amastigotes
Normalized Paraistes per RAW cell
n.s.
n.s.
DMSO
Entospletinib
DMSO
Entospletinib
E
BMDM – L. amazonensis
Promastigotes
Amastigotes
Normalized Paraistes per Mϕ
n.s.
n.s.
p = 0.07
DMSO
Entospletinib
DMSO
Entospletinib

Figure 3

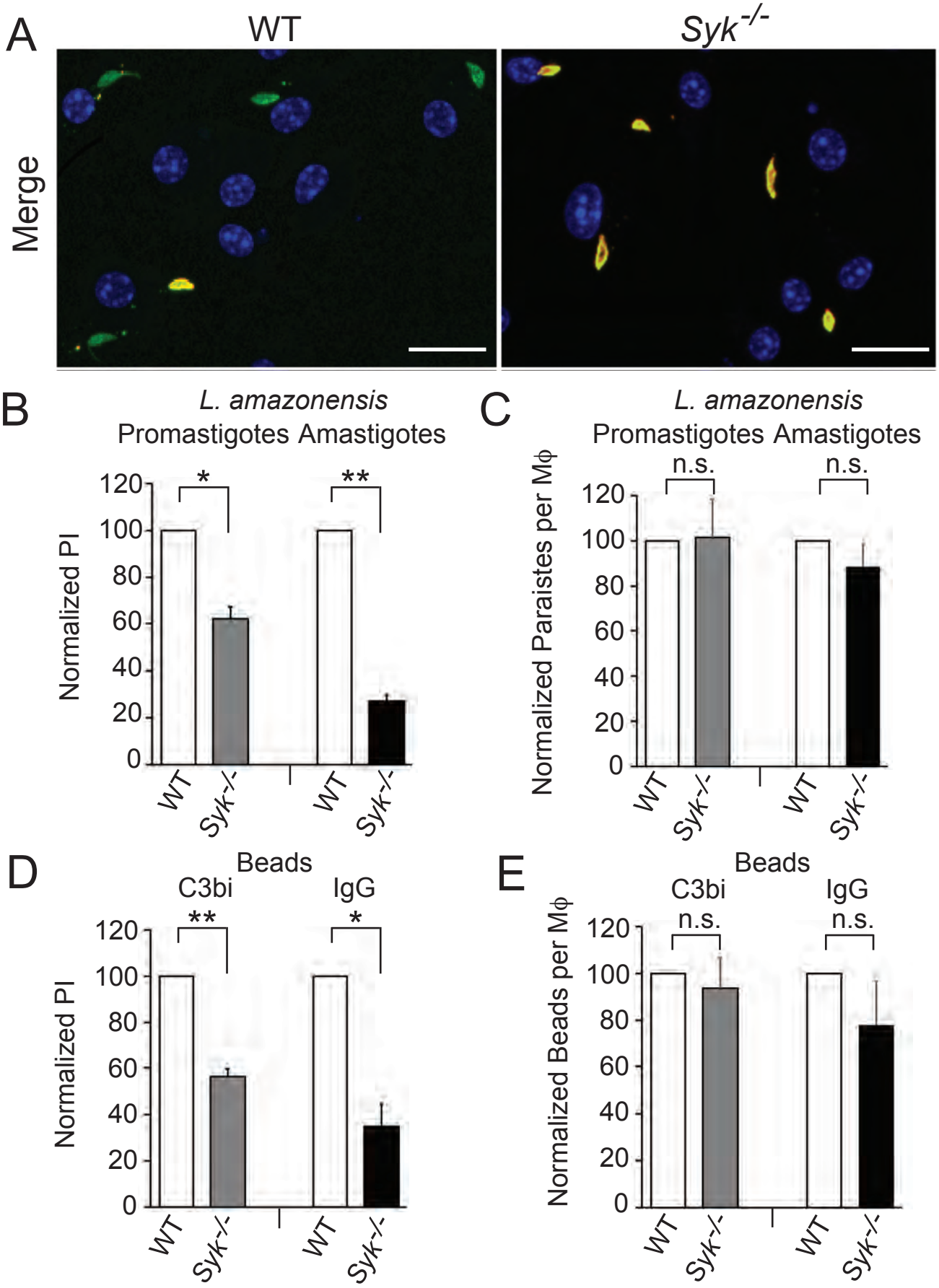
A
WT
Syk-/-
Merge
B
L. amazonensis
Promastigotes Amastigotes
Normalized PI
120
100
80
60
40
20
0
*
**
WT
Syk-/-
WT
Syk-/-
C
L. amazonensis
Promastigotes Amastigotes
Normalized Paraistes per Mϕ
n.s.
n.s.
120
100
80
60
40
20
0
WT
Syk-/-
WT
Syk-/-
D
Beads
C3bi
IgG
Normalized PI
**
*
120
100
80
60
40
20
0
WT
Syk-/-
WT
Syk-/-
E
Beads
C3bi
IgG
Normalized Beads per Mϕ
n.s.
n.s.
120
100
80
60
40
20
0
WT
Syk-/-
WT
Syk-/-

Figure 4

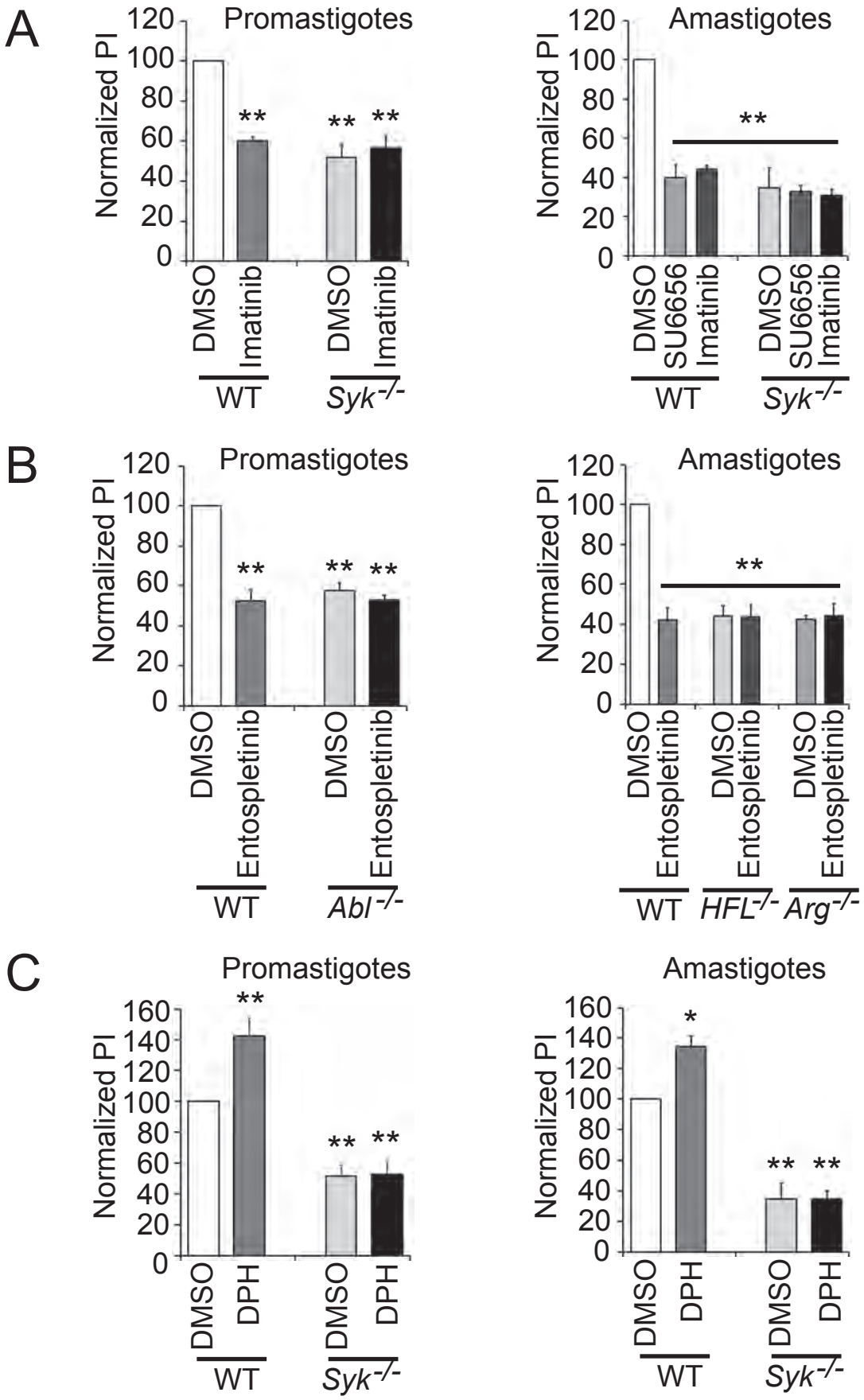
A
Promastigotes
Amastigotes
Normalized PI
120
100
80
60
40
20
0
**
DMSO
Imatinib
SU6656
WT
Syk-/-
B
Entospletinib
Abl-/-
HFL-/-
Arg-/-
C
DPH
*

Figure 5

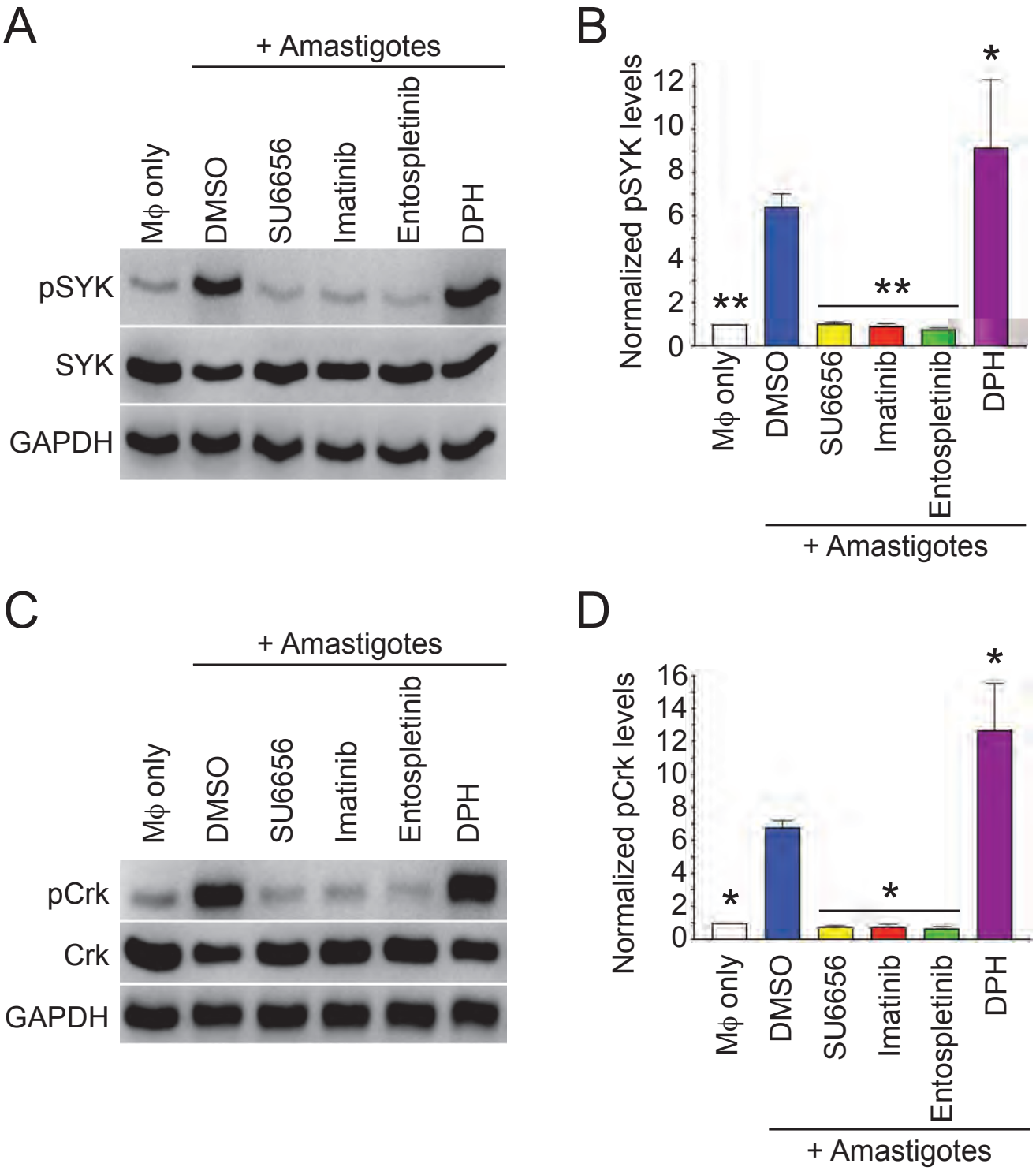
A
+ Amastigotes
Mϕ only
DMSO
SU6656
Imatinib
Entospletinib
DPH
pSYK
SYK
GAPDH
B
Normalized pSYK levels
12
10
8
6
4
2
0
**
**
*
Mϕ only
DMSO
SU6656
Imatinib
Entospletinib
DPH
+ Amastigotes
C
+ Amastigotes
Mϕ only
DMSO
SU6656
Imatinib
Entospletinib
DPH
pCrk
Crk
GAPDH
D
Normalized pCrk levels
16
14
12
10
8
6
4
2
0
*
*
*
Mϕ only
DMSO
SU6656
Imatinib
Entospletinib
DPH
+ Amastigotes

Figure 6

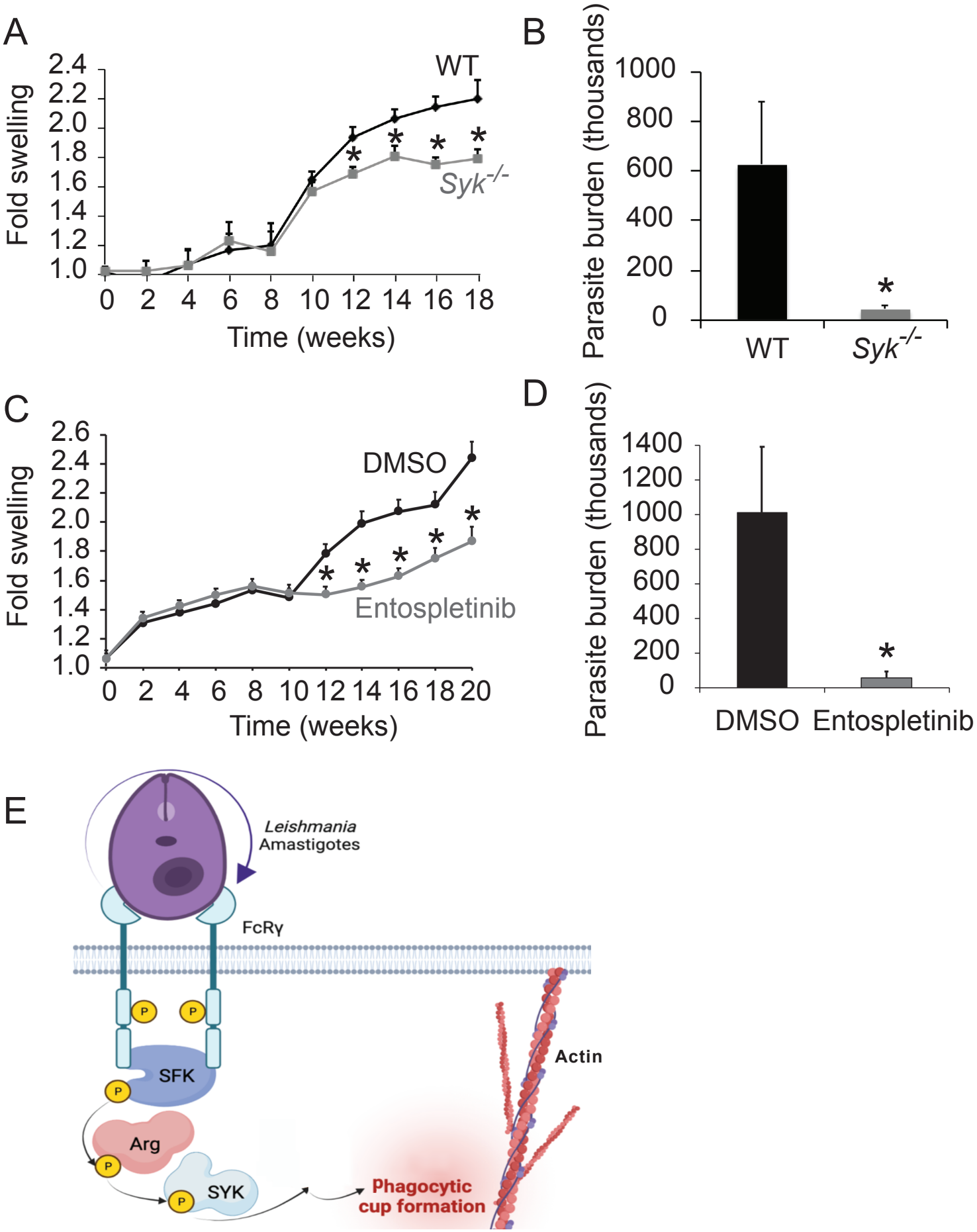
A
Fold swelling
2.4
2.2
2.0
1.8
1.6
1.4
1.2
1.0
WT
Syk-/-
0 2 4 6 8 10 12 14 16 18
Time (weeks)
B
Parasite burden (thousands)
1000
800
600
400
200
0
WT
Syk-/-
C
Fold swelling
2.6
2.4
2.2
2.0
1.8
1.6
1.4
1.2
1.0
DMSO
Entospletinib
0 2 4 6 8 10 12 14 16 18 20
Time (weeks)
D
Parasite burden (thousands)
1400
1200
1000
800
600
400
200
0
DMSO
Entospletinib
E
Leishmania
Amastigotes
FcRγ
P
SFK
Arg
SYK
Actin
Phagocytic
cup formation

764 **FIGURE LEGENDS**

765 **Fig. 1. The SYK inhibitor entospletinib decreases C3bi and IgG-mediated**
766 **phagocytosis**. Mϕs were treated with 1 μM entospletinib or DMSO for 2 h and incubated
767 with C3bi or IgG-coated beads for 30 m. A multi-colored immunofluorescence assay was
768 used to distinguish between extracellular (red + green) and intracellular (green) beads
769 (see methods for details). Nuclei are labeled with Hoescht 33258. (A) Image of anti-P8
770 C3bi-opsonized bead uptake by RAW 264.7 cells treated with DMSO (top) or
771 entospletinib (bottom). Scale bar = 10 μm. In the top panel, there are portions of 12 Mϕ
772 nuclei visible, with 21 total beads and 7 external beads (*i.e.,* 14 internalized beads),
773 suggesting a phagocytic index (PI) of 117. In the bottom panel, 11 Mϕ nuclei are seen,
774 with 20 total beads and 16 extracellular beads (*i.e.,* 4 intracellular amastigotes),
775 suggesting a PI of 36. (B) Quantification of the effects of entospletinib on C3bi-coated
776 and IgG-coated bead uptake by RAW 264.7 cells. Shown is the mean PI ± SE for RAW
777 cells incubated in 1 μM entospletinib and allowed to take up C3bi-coated (left) or IgG-
778 coated beads (right), normalized to RAW cells incubated in an equivalent volume of
779 DMSO and the same number of beads (shown as PI = 100%). (C) Enumeration of the
780 effect of entospletinib on C3bi-coated and IgG-coated bead uptake by BMDM. Shown is
781 the mean PI ± SE, calculated through the methodology described in (B). (D, E)
782 Entospletinib does not affect the total number of C3bi- and IgG-coated beads bound to
783 (D) RAW 264.7 cells and (E) BMDM. Shown is the total number of beads per Mϕ ± SE
784 after Mϕ were incubated in 1 μM entospletinib and allowed to take up C3bi-coated (left)
785 or IgG-coated beads (right), normalized to Mϕ incubated in an equivalent volume of

786 DMSO and beads. For B-E: n = 3 separate experiments; *$p < 0.05$, **$p < 0.01$ (one sample
787 t-test).
788
789 **Fig. 2. The SYK inhibitor entospletinib decreases *Leishmania* uptake**. Mϕ were
790 treated with entospletinib or DMSO for 2 h and incubated with C3bi-coated *L.*
791 *amazonensis* promastigotes or IgG-coated *L. amazonensis* amastigotes for 30 m.
792 Immunofluorescence was used to distinguish between extracellular (red + green) and
793 intracellular (green) promastigotes or amastigotes. Mϕ nuclei are labeled with Hoescht
794 33258. (A) Image of anti-P8 IgG-opsonized amastigote uptake by RAW 264.7 cells
795 treated with DMSO (top) or entospletinib (bottom). Scale bar = 5 μm. In the top panel
796 there are portions of 5 Mϕ nuclei visible, with 7 total amastigotes and 2 external
797 amastigotes (*i.e.,* 5 internalized amastigotes), suggesting a PI of 100. In the bottom panel,
798 4 Mϕ nuclei are seen, with 7 total amastigotes and 5 extracellular amastigotes (*i.e.,* 2
799 intracellular amastigotes), suggesting a PI of 50. (B, C) Quantification of the effects of
800 entospletinib on promastigote or amastigote uptake by (B) RAW 264.7 cells and (C)
801 BMDM. Shown is the PI ± SE for Mϕ incubated in 1 μM entospletinib and allowed to take
802 up promastigotes (left) or amastigotes (right), normalized to Mϕ incubated in an equivalent
803 volume of DMSO and the same number of beads. (D, E) Entospletinib does not affect the
804 total number of promastigotes and amastigotes bound to (D) RAW 264.7 cells and (E)
805 BMDM. Shown is the total number of parasites per Mϕ ± SE after Mϕ were incubated in 1
806 μM entospletinib and allowed to take up promastigotes (left) or amastigotes (right),
807 normalized to Mϕ incubated in an equivalent volume of DMSO and the same number of
808 parasites. n = 3 separate experiments; *$p < 0.05$, **$p < 0.01$ (one sample t-test).

809

810 **Fig. 3. BMDM lacking SYK exhibit defects in C3bi- and IgG-mediated phagocytosis**
811 **and *L. amazonensis* uptake.** (A) Merged image of promastigote uptake by WT BMDM
812 (left) or *Syk*$^{flox/flox}$ LysM Cre+ BMDM (*Syk*$^{-/-}$ BMDM, right), using the methodology
813 described in Fig 2. Scale bar = 10 μm. On the left of this representative image, there are
814 8 full Mϕ nuclei visible, with 5 total promastigotes and 4 internalized promastigotes,
815 suggesting a PI of 50. On the right, 7 Mϕ nuclei are seen, with 5 total promastigotes and
816 0 intracellular promastigotes. (B) *Syk*$^{-/-}$ BMDM exhibit defects in promastigote and
817 amastigote uptake. BMDM were incubated with *L. amazonensis* promastigotes or
818 amastigotes as in Fig 2. Graph shows the mean PI ± SE for promastigotes and
819 amastigotes for *Syk*$^{-/-}$ BMDM, normalized to WT BMDM, using the methodology
820 described in Fig. 2. (C) Mean normalized total number of promastigotes or amastigotes
821 bound to *Syk*$^{-/-}$ BMDM, normalized to WT BMDM, ± SE. (D) *Syk*$^{-/-}$ BMDM are less able
822 to undergo C3bi and IgG-mediated phagocytosis. BMDM were incubated with C3bi or
823 IgG-coated beads as in Fig. 1. Shown is the mean PI ± SE for beads taken up by *Syk*$^{-/-}$
824 BMDM, normalized to WT BMDM (using the methodology described in Fig. 1). (E) Mean
825 normalized total number of C3bi or IgG-coated beads bound to *Syk*$^{-/-}$ BMDM, normalized
826 to WT BMDM, ± SE. n = 3 separate experiments; *p<0.05, **p<0.01 (one sample t-test).
827

828 **Fig. 4. A SFK-Abl/Arg-SYK signaling pathway facilitates *Leishmania* uptake.** (A)
829 Treating *Syk*$^{-/-}$ BMDM with SU6656 or imatinib does not further diminish *Leishmania*
830 promastigote (left) or amastigote uptake (right). (B) Entospletinib has no effect on
831 promastigote uptake by BMDM lacking Abl (left) or amastigote uptake by BMDM lacking

832 Hck, Fgr, and Lyn or Arg kinases (right). (C) The Arg/Abl activator DPH does not rescue
833 *Leishmania* promastigote (left) or amastigote uptake (right) in *Syk*$^{-/-}$ BMDM. For all
834 categories, BMDM of the genotypes shown were incubated with DMSO, SU6656,
835 imatinib, entospletinib, or DPH as indicated and allowed to take up promastigotes or
836 amastigotes. PIs were calculated and values were normalized to WT, DMSO treated
837 BMDM (100%). Mean ± SE shown. n = 3 separate biological experiments; *p<0.05,
838 **p<0.01 by ANOVA compared to WT DMSO treated Mϕ.
839
840 **Fig. 5. SYK is activated by SFK/Arg and phosphorylates downstream effectors**
841 **during amastigote uptake.** (A, B) SYK phosphorylation is decreased by inhibition of SFK
842 or Abl family kinases and increased by activating Abl family kinases. RAW 264.7 cells
843 treated with DMSO or inhibitors were incubated with IgG-coated amastigotes (*i.e.*, +
844 amastigotes) for 15 m before processing for immunoblotting. (A) Representative
845 immunoblot of pSYK (top) and total SYK (middle) in DMSO-treated RAW 264.7 cells (±
846 amastigotes) and amastigote-stimulated SU6656, imatinib, entospletinib, or DPH-treated
847 RAW 264.7 cells. GAPDH (bottom) is used as an additional loading control. (B) Graph
848 presents relative pSYK levels, normalized to SYK levels, among RAW 264.7 cell
849 categories shown in (A). pSYK/SYK levels for Mϕs only (*i.e.*, no amastigotes) were
850 normalized to 1. (C, D) Phosphorylation of the SFK/Abl/Arg substrate CrkII (pCrk) induced
851 upon amastigote uptake is decreased in entospletinib-treated Mϕs. (C) Representative
852 immunoblot of pCrk (top) and total CrkII (middle) in DMSO-treated RAW 264.7 cells (±
853 amastigotes) and amastigote-stimulated SU6656, imatinib, entospletinib, or DPH-treated
854 RAW 264.7 cells. GAPDH is used as an additional loading control. (D) Relative levels for

855 pCrk, normalized to CrkII, graphed as in B. For all categories, n = 4 separate biological
856 experiments; mean ± standard deviations shown. *$p < 0.05$, **$p < 0.01$ by ANOVA
857 compared to pSYK or pCrk levels in WT DMSO-treated Mϕ incubated with amastigotes.
858
859 **Fig. 6. SYK facilitates efficient infection in a mouse model of cutaneous**
860 **leishmaniasis.** (A) Comparison of lesion size in WT versus *Syk*$^{flox/flox}$ LysM Cre+ mice.
861 10 mice per category were infected in the right hind foot with 1 X 10^6 *L. amazonensis*
862 metacyclic promastigotes and monitored over time. Three experiments were performed;
863 shown is a representative experiment. Graphed are the mean ± SE increase in infected
864 foot width when compared to the uninfected foot. *$p < 0.05$ by ANOVA compared to WT
865 mice. (B) *Syk*$^{flox/flox}$ LysM Cre+ mice have a lower parasite burden than WT mice. Plotted
866 is the mean number of parasites isolated from lesions in millions at the termination of (A)
867 at wk 18, ± SE. *$p < 0.05$ by *t*-test. (C) Comparison of lesion size in DMSO/diluent vs.
868 entospletinib-treated mice. Experiment performed as in (A), except that mice were treated
869 with 100 mg/kg/d of entospletinib in their drinking water or the equivalent volume of
870 diluent, starting 4 days prior to infection and continuing throughout the experiment. *$p <$
871 0.05 by ANOVA compared to DMSO-treated mice. (D) Entospletinib-treated mice have a
872 lower parasite burden than DMSO-treated mice. Shown is the mean number of *L.*
873 *amazonensis* parasites in millions isolated from infected footpads at the termination of (C)
874 at wk 20, calculated as in (B), ± SE. *$p < 0.05$ by *t*-test. (E) Relationship between FcR
875 signaling, SFKs, Arg, and SYK during *Leishmania* amastigote uptake. Upon FcRγ ligation
876 by amastigotes, host cell Hck, Fgr, and Lyn are activated. These SFKs phosphorylate
877 and activate Arg kinase, which phosphorylates and activates SYK. SYK activates other

878 kinases within the host cell (*e.g.,* CrkII), leading to actin polymerization and parasite
879 uptake. Diagram created with Biorender (https://www.biorender.com).
880
881 **Table 1. Cytokine secretion in WT vs *Syk$^{flox/flox}$* LysM Cre+ mice** (abbreviated in the
882 table as *Syk$^{-/-}$*). In general, cytokine secretion after *Leishmania* antigen stimulation is not
883 significantly affected in *Syk$^{flox/flox}$* LysM Cre+ mice. The exception is secretion of IL1-β,
884 for which SYK activity is known to be required. Shown are mean ± SE of cytokine profiles
885 of draining lymph nodes isolated from the WT versus *Syk$^{flox/flox}$* LysM Cre+ mice at the
886 end of the experiment shown in Fig 6, with *p* values calculated by Student's *t*-test. 5 x
887 10^6 cells were cultured for 72 h in medium alone (unstimulated, resulting in values that
888 were negligible), or with the addition of lysates made from 2.5 x 10^6 (high stimulation) or
889 from 5 x 10^5 (low stimulation) *L. amazonensis* parasites. Concanamycin A (Con A) was
890 used as a positive control for stimulation. Media was harvested and used in ELISAs for
891 the above-listed cytokines as described previously (Wetzel *et al.*, 2012; Wetzel *et al.*,
892 2016).
893
894 **Table 2. Culturing draining lymph nodes with entospletinib does not affect cytokine**
895 **secretion.** Isolated draining lymph nodes from 4 infected DMSO-treated mice were
896 cultured as described as in Table 1, except that either DMSO or 2 μM entospletinib was
897 added to each of these 4 isolated draining lymph nodes during culture for 72 h. Cytokine
898 ELISAs were performed on harvested supernatants as in Table 1. Mean ± SE shown,
899 with *p* values calculated by Students *t*-test. The lone statistically significant result (IL-13,
900 high stimulation) is the opposite of the result that would be expected if immunological

901 effects facilitated healing in entospletinib-treated mice (Jones *et al.*, 1998).

902

903 **Table 1**

Cytokine	Genotype	Cytokine secretion (pg) after		
		High stimulation	**Low stimulation**	**Con A stimulation**
IL-1β	WT	1,226 ± 91	864 ± 86	1,160 ± 132
	Syk$^{-/-}$	604 ± 55	735 ± 51	750 ± 55
	p	0.000039	0.19	0.0068
IFN-γ	WT	13,044 ± 3,307	9,950 ± 1,344	16,295 ± 3,659
	Syk$^{-/-}$	16,006 ± 3,383	12,084 ± 2,146	14,059 ± 2,088
	p	0.56	0.45	0.59
IL-4	WT	1,094 ± 146	1,093 ± 213	1,168 ± 97
	Syk$^{-/-}$	1,485 ± 240	1,237 ± 172	1,631 ± 364
	p	0.20	0.60	0.30
IL-10	WT	973 ± 292	1,666 ± 516	1,285 ± 433
	Syk$^{-/-}$	1,547 ± 428	990 ± 241	2,091 ± 656
	p	0.30	0.22	0.35
IL-13	WT	824 ± 262	475 ± 104	396 ± 76
	Syk$^{-/-}$	596 ± 119	498 ± 75	616 ± 84
	p	0.41	0.85	0.075
IL-17	WT	< 156	< 156	< 156
	Syk$^{-/-}$	< 156	< 156	< 156
TNF-α	WT	< 124	< 124	< 124
	Syk$^{-/-}$	< 124	< 124	< 124

904

905

906 **Table 1. Cytokine secretion in WT vs *Syk*$^{flox/flox}$ LysM Cre+ mice** (abbreviated in the

907 table as *Syk*$^{-/-}$).

908

909 **Table 2**

Cytokine	Treatment	Cytokine secretion (pg)	
		High stimulation	**Low stimulation**
IFN-γ	DMSO	10,274 ± 509	13,455 ± 3,689
	Entospletinib	14,140 ± 4,374	19,226 ± 5,478
	p	n.s.	n.s.
IL-4	DMSO	1,522 ± 239	1,183 ± 511
	Entospletinib	1,047 ± 222	832 ± 187
	p	n.s.	n.s.
IL-10	DMSO	1,631 ± 442	2,013 ± 820
	Entospletinib	2,664 ± 424	2,451 ± 657
	p	n.s.	n.s.
IL-13	DMSO	342 ± 34.5	330 ± 36.6
	Entospletinib	491 ± 20.3	452 ± 53.2
	p	0.021	n.s.

910

911 **Table 2. Culturing draining lymph nodes with entospletinib does not affect cytokine**

912 **secretion.**

Figure S1

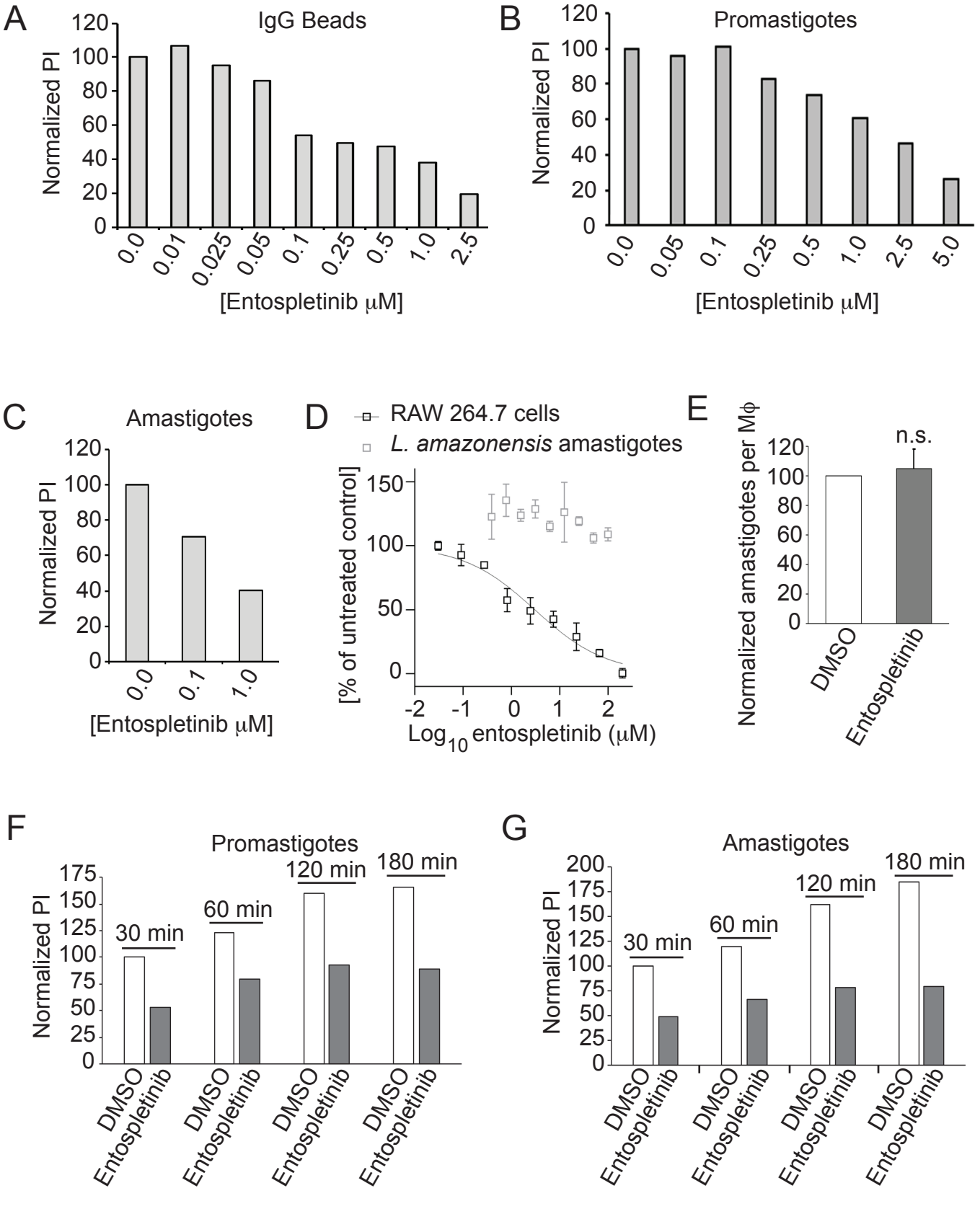
A
IgG Beads
Normalized PI
120
100
80
60
40
20
0
0.0
0.01
0.025
0.05
0.1
0.25
0.5
1.0
2.5
[Entospletinib μM]
B
Promastigotes
Normalized PI
0.0
0.05
0.1
0.25
0.5
1.0
2.5
5.0
[Entospletinib μM]
C
Amastigotes
Normalized PI
0.0
0.1
1.0
[Entospletinib μM]
D
RAW 264.7 cells
L. amazonensis amastigotes
[% of untreated control]
150
100
50
0
-2
-1
0
1
2
Log10 entospletinib (μM)
E
Normalized amastigotes per Mϕ
n.s.
DMSO
Entospletinib
F
Promastigotes
Normalized PI
175
150
125
100
75
50
25
0
30 min
60 min
120 min
180 min
DMSO
Entospletinib
G
Amastigotes
Normalized PI
200
175
150
125
100
75
50
25
0
30 min
60 min
120 min
180 min
DMSO
Entospletinib

Fig. S1. Titrations of entospletinib dosage and effects over time. (A) Titration of entospletinib's effects on IgG-coated bead uptake by RAW 264.7 cells. Mϕs were treated with DMSO (shown as 0.0 μM entospletinib) or increasing concentrations of entospletinib for 2 h and incubated with IgG-coated beads for 30 m. Shown is one representative experiment of 2 experiments. Data normalized to DMSO category (PI = 100%). (B) Titration of entospletinib's effects on promastigote uptake by RAW 264.7 cells. Mϕs were treated with increasing concentrations of entospletinib or DMSO for 2 h and incubated with IgG-coated amastigotes for 30 m. Shown is one representative experiment of 2 experiments. (C) Titration of entospletinib's effects on amastigote uptake by RAW 264.7 cells. Mϕs were treated with DMSO, 0.1 μM, or 1 μM entospletinib and incubated with IgG-coated amastigotes for 30 m. Shown is one representative experiment of 2 experiments. (D) Entospletinib log concentration-response curves for RAW 264.7 cells (black) and axenic *L. amazonensis* amastigotes (grey) for one representative experiment of 3 biological replicate experiments. Triplicate technical replicates were used. Cells were incubated for 72 h in the concentrations of entospletinib shown. (E) Treatment with 0.5 μM entospletinib has no effects on *L. amazonensis* amastigote survival inside RAW 264.7 cells. Mϕs were allowed to internalize *L. amazonensis* amastigotes expressing mNeonGreen, and then, after 24 h, they were incubated with DMSO or 0.5 μM entospletinib for 72 h. Shown is the mean number of *L. amazonensis* amastigotes per 100 entospletinib-treated Mϕ, normalized to DMSO-treated Mϕ (100%), ± SE. n = 3 separate biological replicates. (F) The relative decrease in promastigote PI in entospletinib-treated RAW 264.7 cells does not change after long drug incubations. Mϕs were treated with 1 μM entospletinib or DMSO for 2 h and incubated with C3bi-coated

promastigotes for 30, 60, 120, or 180 m. Data normalized to DMSO, 30 m category. Shown is one representative experiment of 2 experiments. (G) The relative decrease in amastigote PI in entospletinib-treated RAW 264.7 cells does not change after long drug incubations. Experiment performed as in (F), except that Mϕs were incubated with IgG-opsonized amastigotes. Shown is one representative experiment of 2 experiments.

Figure S2

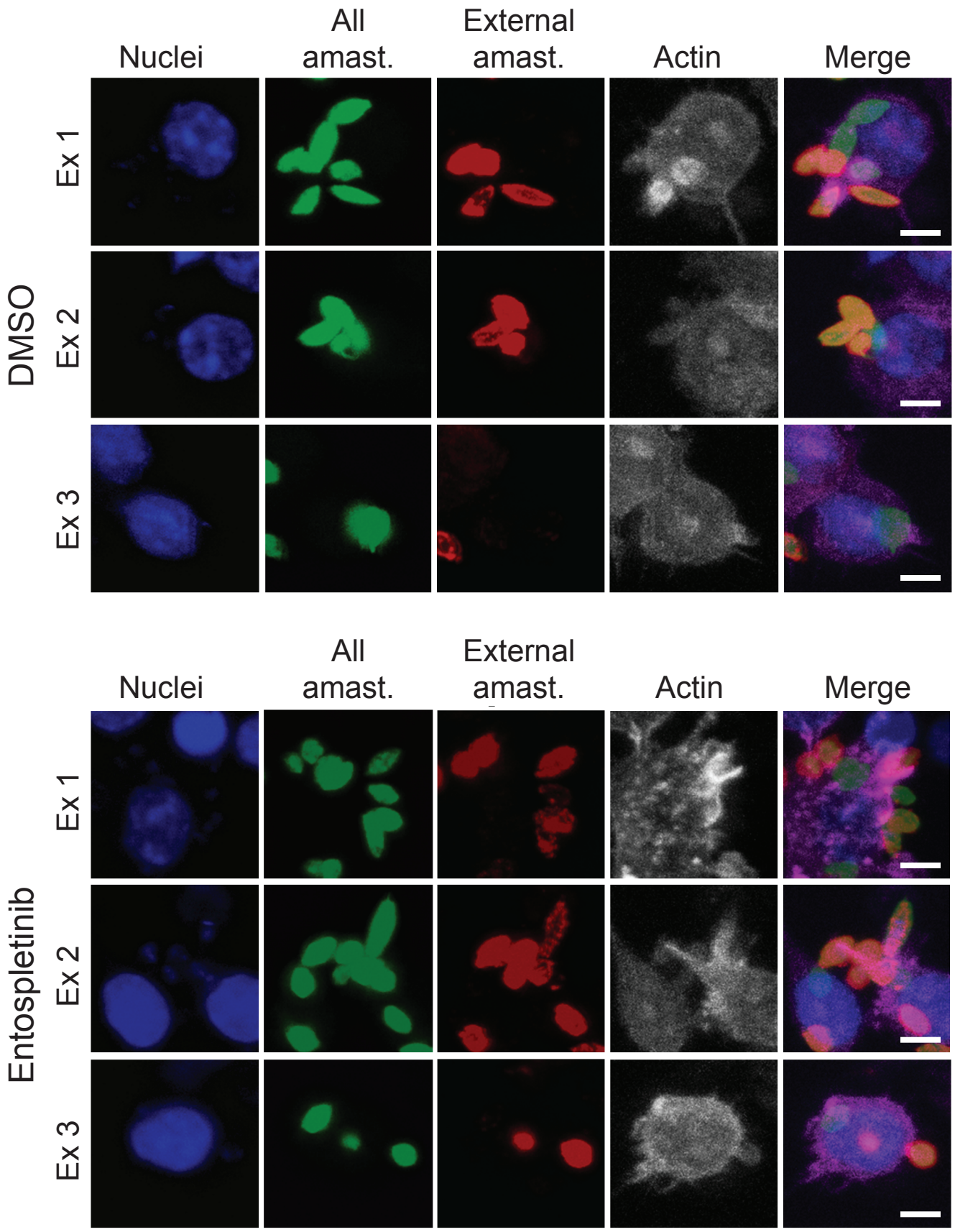
Nuclei
All amast.
External amast.
Actin
Merge
DMSO
Ex 1
Ex 2
Ex 3
Nuclei
All amast.
External amast.
Actin
Merge
Entospletinib
Ex 1
Ex 2
Ex 3

Fig. S2. Representative phagocytic cups in DMSO vs entospletinib-treated Mϕs taking up *Leishmania* amastigotes. Shown are three separate examples of phagocytic cups in DMSO versus entospletinib-treated RAW 264.7 cells that are in the process of internalizing amastigotes. From left to right: Mϕ nuclei (blue, Hoescht); all amastigotes (green; p8); external amastigotes (red); actin (white/pink; phalloidin). Scale bar = 2 μm. Circular phagocytic cups like those seen in example 1 in the DMSO-treated Mϕs were not seen in entospletinib-treated Mϕs, consistent with prior literature suggesting that there are defects in cup closure in *SYK*$^{-/-}$ Mϕs (Crowley *et al.*, 1997). Actin staining also appears brighter in entospletinib-treated Mϕs than DMSO-treated Mϕs (quantified in Fig. S3B).

Figure S3

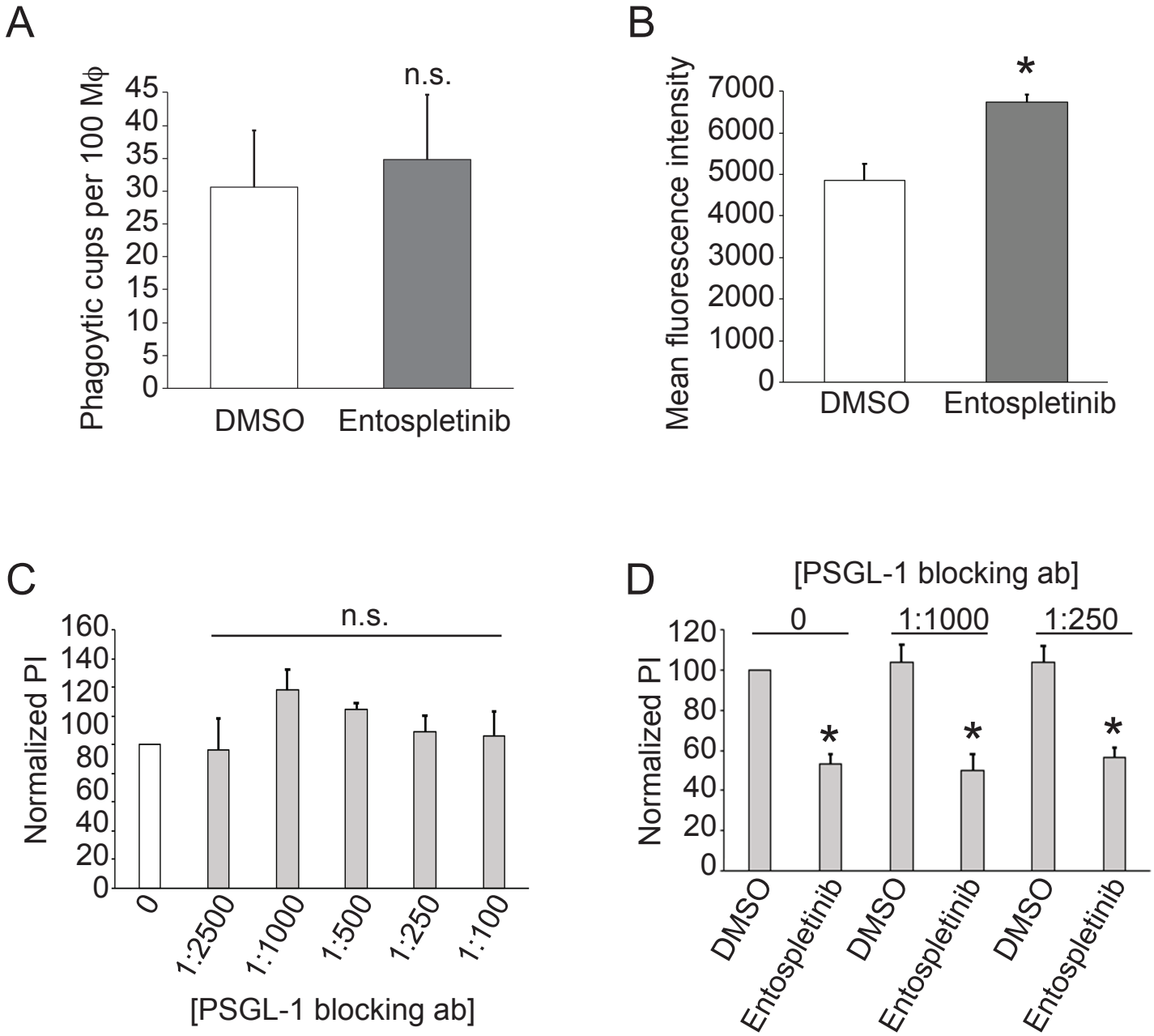
A
Phagoytic cups per 100 Mϕ
45
40
35
30
25
20
15
10
5
0
n.s.
DMSO
Entospletinib
B
Mean fluorescence intensity
7000
6000
5000
4000
3000
2000
1000
0
*
DMSO
Entospletinib
C
Normalized PI
160
140
120
100
80
60
40
20
0
n.s.
0
1:2500
1:1000
1:500
1:250
1:100
[PSGL-1 blocking ab]
D
[PSGL-1 blocking ab]
0
1:1000
1:250
Normalized PI
120
100
80
60
40
20
0
*
*
*
DMSO
Entospletinib
DMSO
Entospletinib
DMSO
Entospletinib

Fig. S3. Mechanisms of SYK signaling during *Leishmania* uptake. (A) Despite differences in PI, the number of phagocytic cups seen between entospletinib-treated and DMSO-treated RAW 264.7 cells incubated with amastigotes is the same. This result is consistent with prior literature documenting defects in phagocytic cup closure (not formation) in *Syk*$^{-/-}$ phagocytes. (B) Actin in phagocytic cups shown in Fig. S2 is brighter in entospletinib-treated Mϕs than in DMSO-treated Mϕs. Relative fluorescence intensity was quantified in ImageJ by an observer blinded to experimental category. Shown is the mean intensity per field among at least 5 fields per category ± SE. *, $p < 0.05$ by *t*-test. (C) Incubation with 4RA10, an antibody to P-selectin glycoprotein ligand 1 (PSGL-1), does not affect uptake of *Leishmania* amastigotes by Mϕs. Mϕs were treated with increasing concentrations of 4RA10 for 2 h and incubated with IgG-coated amastigotes for 30 m to allow internalization as described above. Shown is the mean PI ± SE from 3 biological replicates. All categories non-significant by ANOVA. (D) The entospletinib-induced reduction in amastigote PI is not affected by 4RA10. Mϕs were treated with increasing concentrations of 4RA10 and DMSO vs 1 μM entospletinib for 2 h, then incubated with IgG-coated amastigotes for 30 m to allow internalization as described above. Shown is the mean PI ± SE from 3 biological replicates. *, $p < 0.05$ by ANOVA.

Figure S4

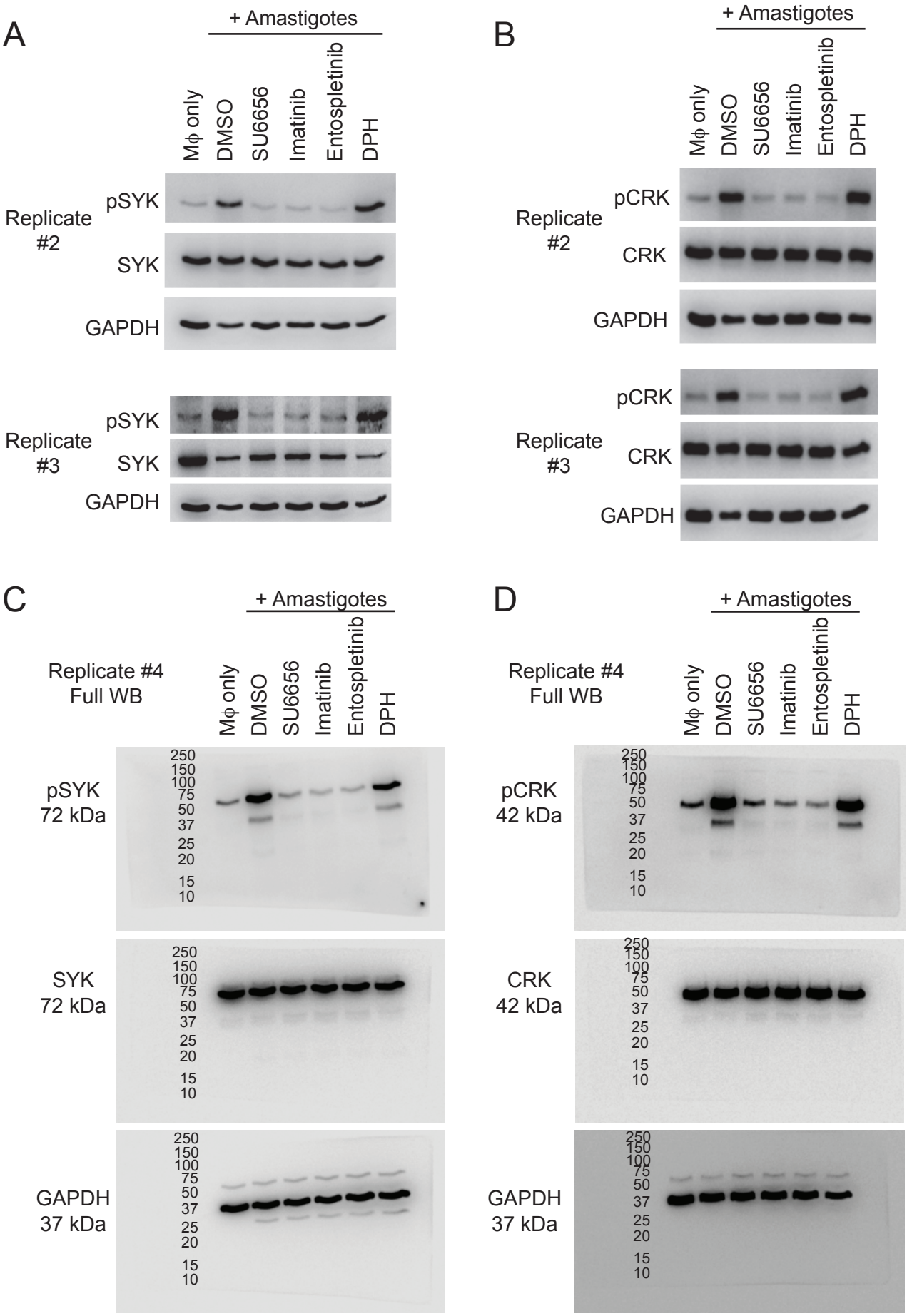
A
+ Amastigotes
Mϕ only
DMSO
SU6656
Imatinib
Entospletinib
DPH
Replicate #2
pSYK
SYK
GAPDH
Replicate #3
pSYK
SYK
GAPDH
B
+ Amastigotes
Mϕ only
DMSO
SU6656
Imatinib
Entospletinib
DPH
Replicate #2
pCRK
CRK
GAPDH
Replicate #3
pCRK
CRK
GAPDH
C
+ Amastigotes
Replicate #4
Full WB
Mϕ only
DMSO
SU6656
Imatinib
Entospletinib
DPH
pSYK
72 kDa
SYK
72 kDa
GAPDH
37 kDa
250
150
100
75
50
37
25
20
15
10
D
+ Amastigotes
Replicate #4
Full WB
Mϕ only
DMSO
SU6656
Imatinib
Entospletinib
DPH
pCRK
42 kDa
CRK
42 kDa
GAPDH
37 kDa
250
150
100
75
50
37
25
20
15
10

Fig. S4. Western Blots. All Western blots quantified in Figure 5 are shown. (A) Biological replicates 2 and 3 of Western blots quantified for pSYK calculations. (B) Biological replicates 2 and 3 of Western blots quantified for pCRK calculations. (C) Full Western blot for biological replicate 4 used for pSYK calculations. (D) Full Western blot for biological replicate 4 used for pCRK calculations.

Figure S5

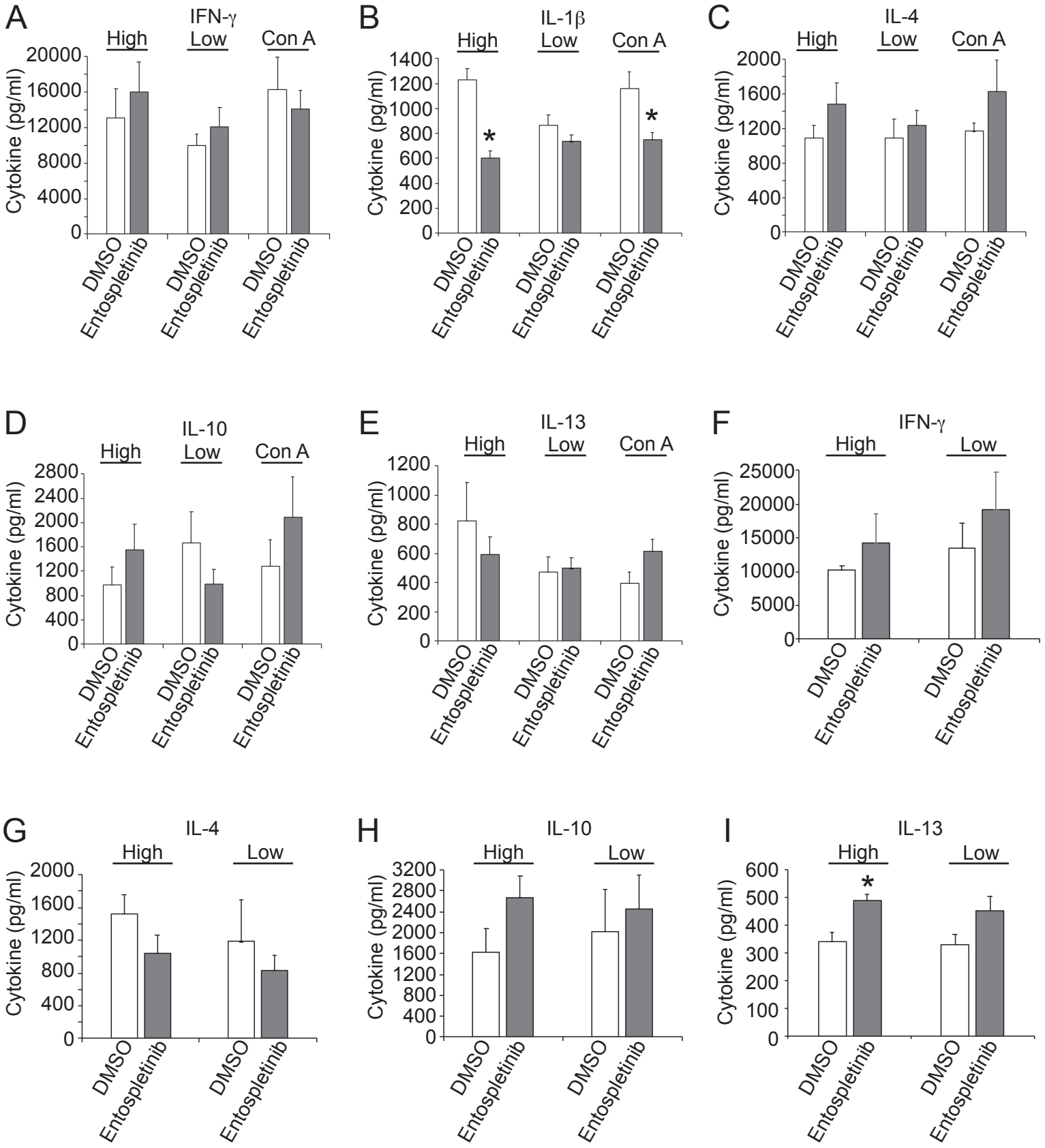
A
IFN-γ
High
Low
Con A
Cytokine (pg/ml)
20000
16000
12000
8000
4000
0
DMSO
Entospletinib
B
IL-1β
High
Low
Con A
Cytokine (pg/ml)
1400
1200
1000
800
600
400
200
0
*
*
DMSO
Entospletinib
C
IL-4
High
Low
Con A
Cytokine (pg/ml)
2000
1600
1200
800
400
0
DMSO
Entospletinib
D
IL-10
High
Low
Con A
Cytokine (pg/ml)
2800
2400
2000
1600
1200
800
400
0
DMSO
Entospletinib
E
IL-13
High
Low
Con A
Cytokine (pg/ml)
1200
1000
800
600
400
200
0
DMSO
Entospletinib
F
IFN-γ
High
Low
Cytokine (pg/ml)
25000
20000
15000
10000
5000
0
DMSO
Entospletinib
G
IL-4
High
Low
Cytokine (pg/ml)
2000
1600
1200
800
400
0
DMSO
Entospletinib
H
IL-10
High
Low
Cytokine (pg/ml)
3200
2800
2400
2000
1600
1200
800
400
0
DMSO
Entospletinib
I
IL-13
High
Low
Cytokine (pg/ml)
600
500
400
300
200
100
0
*
DMSO
Entospletinib

Fig. S5. Graphical representations of cytokine secretion data. (A-E) Graphs of data shown in Table 1, separated out by cytokine. A = IFN-γ, B= IL-1β, C = IL-4, D = IL-10, E = IL-13. (F-I) Graphs of data shown in Table 2, separated out by cytokine. F = IFN-γ, G = IL-4, H = IL-10, I = IL-13. *, $p < 0.05$ by *t*-test.

Table S1. Cytokine secretion is not skewed towards a Th1 or Th2 response during *L. amazonensis* infection of *Syk*$^{flox/flox}$ LysM Cre+ mice compared to WT mice.

Ratio	**WT – High stimulation**	***Syk*$^{-/-}$ – High stimulation**	**WT – Low stimulation**	***Syk*$^{-/-}$ – Low stimulation**
IFNγ:IL-4	11.9	10.8	9.1	9.8
IFNγ:IL-10	13.4	10.4	6.0	12.2
IFNγ:IL-13	21.9	27.0	20.9	24.2
IFNγ: IL-4+10+13	4.9	4.4	3.1	4.4

Table S1. Cytokine secretion is not skewed towards a Th1 or Th2 response during *L. amazonensis* infection of *Syk*$^{flox/flox}$ LysM Cre+ mice compared to WT mice. Ratios of IFNγ:IL-4, IFNγ:IL-10, IFNγ:IL-13, and IFNγ:IL-4+10+13 were calculated from the data shown in Table 1.